Establishment of the quality assurance method based on patient positioning errors for stereotactic volumetric modulated arc therapy for intracranial lesions

(頭蓋内病変に対する定位的強度変調回転放射線治療における患者位置誤差に基づく品質管理法の確立)

鶴田　裕輔

Physica Medica 81 (2021) 245–252

Contents lists available at ScienceDirect

Physica Medica

journal homepage: www.elsevier.com/locate/ejmp

Technical note

Evaluation of intrafractional head motion for intracranial stereotactic radiosurgery with a thermoplastic frameless mask and ceiling-floor-mounted image guidance device

Yusuke Tsuruta [a,b], Manabu Nakata [a], Mitsuhiro Nakamura [b,c,*], Megumi Uto [c], Keiichi Takehana [c], Hideaki Hirashima [c], Takahiro Fujimoto [a], Takashi Mizowaki [c]

[a] Division of Clinical Radiology Service, Kyoto University Hospital, Kyoto 606-8507, Japan
[b] Division of Medical Physics, Department of Information Technology and Medical Engineering, Human Health Sciences, Graduate School of Medicine, Kyoto University, Kyoto 606-8507, Japan
[c] Department of Radiation Oncology and Image-applied Therapy, Graduate School of Medicine, Kyoto University, Kyoto 606-8507, Japan

ARTICLE INFO

Keywords:
Intrafractional head motion
Translation and rotation
Image guidance
6-DOF robotic couch
Frameless mask

ABSTRACT

Purpose: To evaluate intrafractional head motion (IFM) in patients who underwent intracranial stereotactic radiosurgery with the ExacTrac X-ray system (ETX) and a frameless mask.
Methods: A total of 143 patients who completed a pre-treatment examination for IFM were eligible for this study. The frameless mask type B R408 (Klarity Medical & Equipment Co., Ltd., Guangzhou, China), which covers the back of the head, and the entire face, was used for patient immobilization. After the initial 6D correction and first X-ray verification (IFM_1), X-ray verification was performed every 3 min for a duration of 15 min. The IFM_p ($2 \leq p \leq 6$) was calculated as the positional difference from IFM_1. In addition, the inter-phase *IFM* (*IP-IFM*) and IFM_m were calculated. The *IP-IFM* was defined as $|IFM_p - IFM_{p-1}|$, and IFM_m as the difference between the values after all patients were asked to move their heads intentionally with the frameless mask on.
Results: Both translational IFM_p and *IP-IFM* exceeded 1 mm for a single patient, whereas, for all patients, the translational IFM_m values were kept to within 1 mm in all directions. The proportions of the rotational IFM_p, *IP-IFM*, and IFM_m values within 0.5° were greater than 94.4%, 98.6%, and 90.2% for all of the rotational axes, respectively.
Conclusions: A frameless mask achieved highly accurate patient positioning in combination with ETX and a 6°-of-freedom robotic couch; however, a deviation over 1 mm and 0.5° was observed with low frequency. Therefore, X-ray verification and correction are required during treatment.

1. Introduction

Intracranial stereotactic radiosurgery (SRS) is a popular technique used to deliver an ablative dose to a target in either a single or multiple treatments. Accurate patient positioning and stable immobilization are essential for the treatment of intracranial lesions with high precision [1].

Traditionally, patient immobilization devices for intracranial SRS are invasive, such as the fixing of pins to a patient's skull. Recently, image guidance techniques used in clinical practice have evolved. For example, it has been reported that the ExacTrac X-ray system (ETX) (Brainlab, Feldkirchen, Germany), which is a ceiling-floor mounted image guidance device, achieves highly accurate patient positioning [2–5]. One of the most notable advantages of this system is that there is no need to consider any spatial uncertainty caused by the mechanical movement of X-ray tubes and flat panel detectors. A six-degree-of-freedom (6-DOF) robotic couch has also contributed to improving the accuracy of patient positioning [6,7]. In addition, the image fusion algorithm implemented in the ETX system is reported to be reliable and fast [8]. As a result, noninvasive patient immobilization devices, such as a frameless mask (Klarity Medical & Equipment Co., Ltd., Guangzhou, China), are now applicable for image-guided intracranial SRS [9].

However, concerns remain for image-guided intracranial SRS for

* Corresponding author at: Division of Medical Physics, Department of Information Technology and Medical Engineering, Human Health Sciences, Graduate School of Medicine, Kyoto University, Kyoto 606-8507, Japan.
E-mail address: m_nkmr@kuhp.kyoto-u.ac.jp (M. Nakamura).

https://doi.org/10.1016/j.ejmp.2020.12.019
Received 15 September 2020; Received in revised form 17 December 2020; Accepted 25 December 2020
Available online 20 January 2021

patients immobilized with a frameless mask, specifically intrafractional head motion (IFM) during treatment. Although several studies have evaluated IFM, their definition of IFM has been restricted mainly to the positional difference between patients' head motion pre- and post-treatment as calculated from kV X-ray images [6,10,11]. Mangegius et al. stated that X-ray imaging pre- and post-treatment did not precisely quantify intrafractional head displacements during treatment [12]. They examined the intrafractional error at 1.5-minute time intervals and summarized these errors over the duration of the treatment process; however, their data were acquired from only five patients with good performance status. Therefore, their data were not sufficient to draw any generalized conclusions relating to IFM.

As reported previously, we introduced a pretreatment examination for IFM that was defined based on the value immediately after the initial 6-DOF correction, with the patients' IFM monitored subsequently at 3-minute intervals over a duration of 21 min [13]. At our institution, a total of 3–5 arcs (one or two coplanar arcs and two or four non-coplanar arcs) are typically used in intracranial SRS planning. The verification of kV X-ray images is performed just before irradiation of the first arc to maintain a more accurate patient position, and at each couch rotation in order to correct the associated IFM and mechanical uncertainty. As it takes a few minutes to rotate the couch and to verify the X-ray images obtained following each rotation, it is necessary to perform IFM analysis for consecutive verifications as well as at 3-minute intervals.

Recently, single-isocenter volumetric-arc radiation therapy (VMAT) for multiple brain metastases has been used clinically [14]. One of the advantages of single-isocenter VMAT is that it achieves a similar dose distribution to the conventional multi-isocenter technique with a shorter treatment time. In addition to highly accurate translational motion during treatment, rotational IFM should be suppressed to deliver planned doses to multiple intracranial tumors correctly [2,15] because rotational deviation can result in collateral dosimetric effects being applied to targets separate from the isocenter [16–18]. However, there is little literature on rotational IFM. The purpose of this study was to evaluate rotational and translational IFM for patients who underwent intracranial SRS using ETX and a frameless mask.

2. Material and methods

2.1. Patients and patient immobilization

In this study, a total of 145 consecutive patients (70 males, 75 females; median age, 68 years; range: 16–88 years) who underwent intracranial SRS at Kyoto University Hospital between April 2017 and June 2019 were included regardless of performance status, number of tumors, and tumor location. Our retrospective study was approved by the Institutional Review Board of Kyoto University Hospital (approval number: R1167).

A frameless mask of type B R408 (Klarity Medical & Equipment Co., Ltd., Guangzhou, China) was used for all patients. This mask consists of the rear, middle, and top mask, which cover the back of the head, forehead to chin (partially), and the entire face, respectively. Additionally, a simple dental support strip with a width of 3 cm, including in the mask kit, was used as the bite block. This bite block was made of the same material as the frameless mask. The bite block was used for 130 patients, and was not for 15 patients who had clinical problems such as artificial teeth or poor performance status. An overview of a frameless mask is shown in Fig. 1. CT images were acquired using a SOMATOM Definition AS instrument (Siemens, Erlangen, Germany) and were reconstructed using a slice thickness of 1.0 mm.

2.2. Procedure for evaluating the intrafractional motion

For each patient, a pre-treatment examination for IFM was performed several days before the first day of treatment. This examination is standard hospital practice for all patients who are going to undergo intracranial SRS with a frameless mask. Furthermore, all patients were informed about the pre-treatment examination, including the extra visit, imaging dose, and treatment time.

Dedicated dummy treatment plans were created using Eclipse (Varian Medical Systems, Palo Alto, CA, USA) or iPlan (Brainlab). The isocenter of the dummy plan was the same as that of the approved plan. The beam geometry of the dummy plan consisted of a single co-planar arc field with several MUs because it was necessary to perform patient positioning using the ETX system (Brainlab). The dummy plan was not actually delivered to the patients.

Fig. 2 shows the procedure for the pre-treatment examination for IFM. Patient positioning, image registration, and couch correction were performed without couch rotation using ETX. First, initial patient positioning was performed automatically using an infrared reflective marker-based system. Re-positioning of the patients was performed when the rotational deviation exceeded the motion range of the 6-DOF couch under X-ray correction in the following situations: (1) pitch $>\pm2.7^{\circ}$, (2) roll $>\pm4.0^{\circ}$, (3) pitch $>\pm2.0^{\circ}$, and roll $>\pm3.0^{\circ}$. There were no criteria for translation and yaw in the initial patient positioning.

After this setup, a pair of kV X-ray images were acquired at 80 kV and 6.3 mAs using the ETX. These images were matched automatically via digitally reconstructed radiographs (DRRs) created from the planning CT images, and then translational and rotational shift values were calculated by the ETX system. The pixel size of the flat panel detector of the ETX was 0.258 mm at the isocenter [8]. Fig. 3 shows an example of an ETX display at image registration. The skull contour was excluded from the region of interest to avoid incorrect image registration of the head skin in kV X-ray images and the skull contour of DRRs [8]. In addition, the superior dental arch and mandible were excluded because we recognized that these structures have higher mobility compared with the skull contour. The calculated shift values were applied to correct the patient's position using a 6-DOF robotic couch (X-ray correction). Immediately after the initial 6D correction, measurement of the examination time began, and kV X-ray images were reacquired for patient positioning verification (first X-ray verification; phase-1). For X-ray verification, image registration was performed three times to obtain an

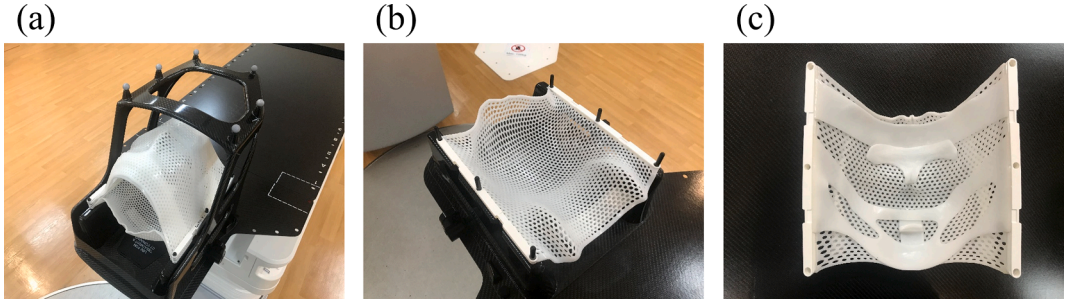

Fig. 1. Example of a frameless mask used in this study. (a) An overview of a frameless mask, (b) rear of the mask, (c) rear view of the front part of the mask, which consists of the middle and front mask sections, and the bite block.

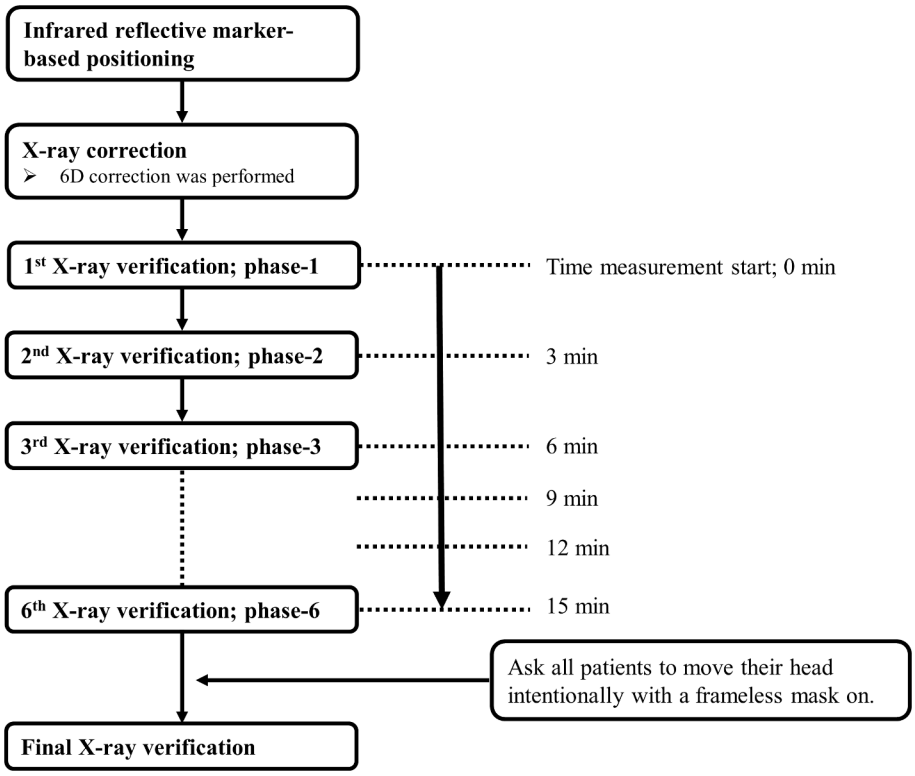

Fig. 2. Procedure for the pre-treatment examination in order to evaluate the intrafractional motion.

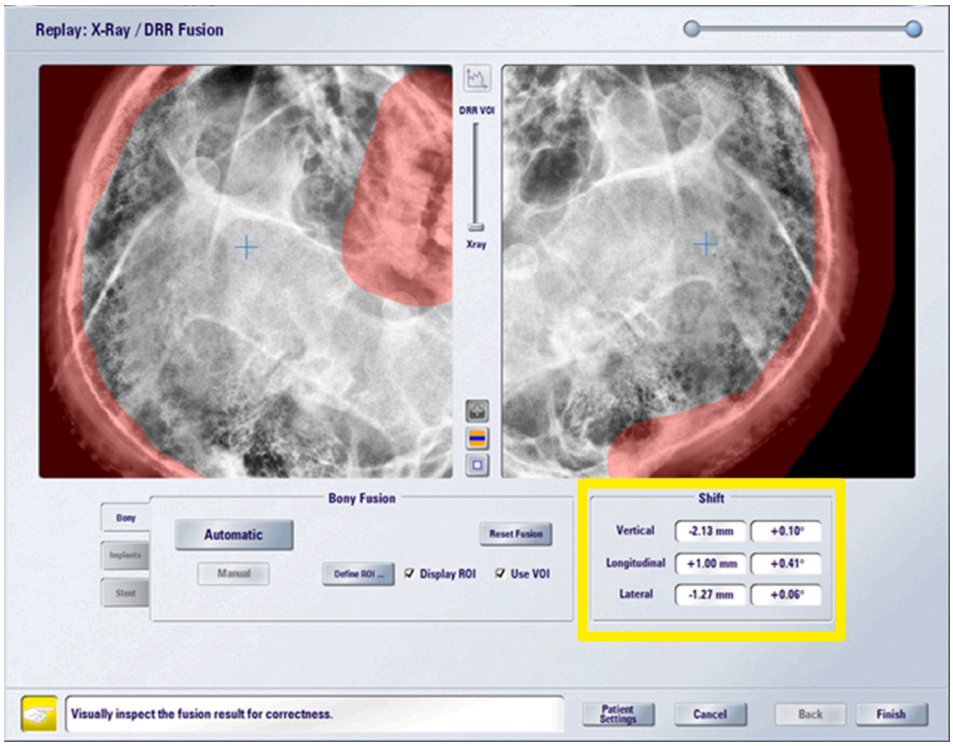

Fig. 3. Example image acquired by the ExacTrac X-ray (ETX) system in actual image registration. The shift values are indicated within the yellow square. The red area in the X-ray images represents the exclusive region for image registration between X-ray images acquired from ETX and digitally reconstructed radiographs. (For interpretation of the references to colour in this figure legend, the reader is referred to the web version of this article.)

average provided by the optimization algorithm implemented in the ETX [19]. The averaged translational and rotational shift values were then recorded as a representative position (6D correction was not performed at this time). The ETX displays the "OK" signal when the shift values were within 0.5 mm and 1.0° for X-ray verification. These values were user-defined thresholds. This procedure was repeated over a period

of 15 min at 3-minute intervals (i.e., until the sixth X-ray verification (phase-6)), which was equivalent to the actual treatment time.

In this study, IFM was defined as the positional difference between the p-th X-ray verification ($2 \le p \le 6$) and the first X-ray verification, as follows:

$$IFM_p^k = V_p^k - V_1^k \quad (1)$$

where k is the number of patients and V_p^k represents the value calculated by the ETX of patient number k at the p-th X-ray verification for each direction (vertical, longitudinal, lateral, yaw, roll, and pitch). Yaw, roll, and pitch denote the rotation about the vertical, longitudinal, and lateral axes, respectively. Fig. 4 shows the definition of translational and rotational deviation from the representative position. The three-dimensional (3D) vector of the translational *IFM* at phase-6 ($^{3D}IFM^k{}_6$) was also calculated:

$$^{3D}IFM_6^k = \sqrt{\left(\ ^{vert}IFM_6^k\right)^2 + \left(\ ^{long}IFM_6^k\right)^2 + \left(\ ^{lat}IFM_6^k\right)^2} \quad (2)$$

where, $^{vert}IFM^k{}_6$, $^{long}IFM^k{}_6$, and $^{lat}IFM^k{}_6$ represent the $IFM^k{}_6$ for the vertical, longitudinal, and lateral axes, respectively.

In addition, the IFM between two consecutive phases (inter-phase *IFM*; *IP-IFM*) was calculated as follows:

$$IP-IFM_{p:p-1}^k = \left|V_p^k - V_{p-1}^k\right| \quad (3)$$

After the sixth X-ray verification (phase-6), all patients were asked by radiation therapists to move their heads intentionally while wearing the frameless mask, and a final X-ray verification was performed. This procedure was intended to understand how stable a frameless mask is in response to intentional motion by a patient. The value of IFM_m was then calculated as follows:

$$IFM_m^k = \left|V_{final}^k - V_6^k\right| \quad (4)$$

where $V^k{}_{final}$ is the value for patient number k at the final X-ray verification calculated by ETX. For comparison with $^{3D}IFM^k{}_6$, the 3D vector of the translational *IFM* at phase-6 ($^{3D}IFM^k{}_m$) was calculated using the following equation:

$$^{3D}IFM_m^k = \sqrt{\left(\ ^{vert}IFM_m^k\right)^2 + \left(\ ^{long}IFM_m^k\right)^2 + \left(\ ^{lat}IFM_m^k\right)^2} \quad (5)$$

where, $^{vert}IFM^k{}_m$, $^{long}IFM^k{}_m$, and $^{lat}IFM^k{}_m$ denote the $IFM^k{}_m$ along the vertical, longitudinal, and lateral axes, respectively.

A paired t-test was performed between $^{3D}IFM_6$ and $^{3D}IFM_m$, with a p-value < 0.05 considered to be statistically significant.

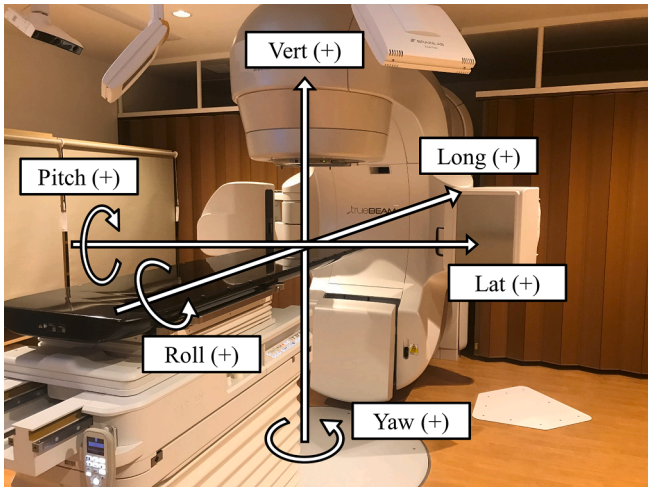

Fig. 4. Schematic showing the translational and rotational directions of the ExacTrac X-ray system.

3. Results

Owing to the compression-related discomfort caused by wearing the frameless mask, two patients did not complete this examination. Therefore, a total of 143 patients were analyzed. Fig. 5 shows histograms of the deviations calculated immediately after the first X-ray verification (phase-1). The translational and rotational deviations were within ±1 mm and ±1°, respectively.

As shown in Fig. 6, the $^{vert}IFM_p$ and $^{long}IFM_p$ values of all patients were within 1 mm irrespective of phase, with an error exceeding 1 mm observed in the $^{lat}IFM_5$ and $^{lat}IFM_6$ measurements for a single patient. The proportion of the rotational *IFM* values within 0.5° was more than 94.4% in any rotational direction. The mean ± standard deviation (SD) of $^{3D}IFM_6$ was 0.28 ± 0.21 mm. The maximum absolute values of the *IFM* were 1.63 mm and 1.33° in phase-6, which were detected in the same patient. The results corresponding to this patient are shown in Fig. 7.

Fig. 8 shows boxplots of the translational and rotational *IP-IFM* and IFM_m values. A movement exceeding 1 mm was observed in the $^{long}IP\text{-}IFM_{3:2}$ for one patient only. The proportion of the *IP-IFM* values within 0.5° was more than 98.6% in any rotational direction. The maximum value of rotation was 0.89° in the $^{Yaw}IP\text{-}IFM_{3:2}$. For all patients, the translational IFM_m values were within 1 mm in all directions, and the mean ± SD values were 0.11 ± 0.09 mm, 0.12 ± 0.11 mm, and 0.10 ± 0.10 mm for the vertical, longitudinal, and lateral axes, respectively. The proportions of the rotational IFM_m values within 0.5° were 90.2%, 95.1%, and 93.0% for the yaw, roll, and pitch, respectively. The mean ± SD of the $^{3D}IFM_m$ in all patients was 0.21 ± 0.14 mm. No statistical significance was observed between $^{3D}IFM_6$ and $^{3D}IFM_m$. Fig. 9 shows the results for the patient who showed the largest motion (1.19 mm) observed in the $^{long}IP\text{-}IFM_{3:2}$. By contrast, the absolute value of the $^{long}IFM_6$ for this patient was 0.13 mm.

4. Discussion

We begin with a discussion of the imaging dose of the ETX, because all patients received additional doses in this pre-treatment examination. When the machine was commissioned, the imaging dose was measured using the same method as Hamada et al. [20]. They reported that the imaging dose from each X-ray tube of the ETX system was 0.086 and 0.088 mGy at 100 kV and 6.3 mAs, respectively. Our experimental measurement of the imaging dose at the isocenter was approximately 0.05 mGy per single kV X-ray image at 80 kV and 6.3 mAs, which was comparable to that reported by Hamada et al. Although the imaging dose at the pre-treatment examination was remarkably low compared to the treatment dose, nevertheless the patients were exposed to an additional dose from eight pairs of kV X-ray images (16 images in total). However, we assert that the pre-treatment examination is required to judge whether the SRS can be safely carried out based on the ALARA principle [21].

Basically, the image fusion by the ETX is considered highly accurate and reliable. However, the image fusion results have a variation of 0.1–0.2 mm and 0.1–0.2° at every image registration. Considering the pixel size of the imager, these variations are inevitable. In order to reduce these variations in the fusion results, for every X-ray verification, image registration was performed three times, and the averaged translational and rotational shift values were recorded as a representative position.

The translational and rotational deviation immediately after the first X-ray verification showed the high accuracy of patient positioning in our study (Fig. 5). Table 1 summarizes the positioning accuracy reported by other groups along with our results. These values were acquired immediately after the initial patient positioning using a 6-DOF robotic couch. Verbakel et al. [11] and Keeling et al. [22] also reported similar results for the patient positioning accuracy using the same equipment as

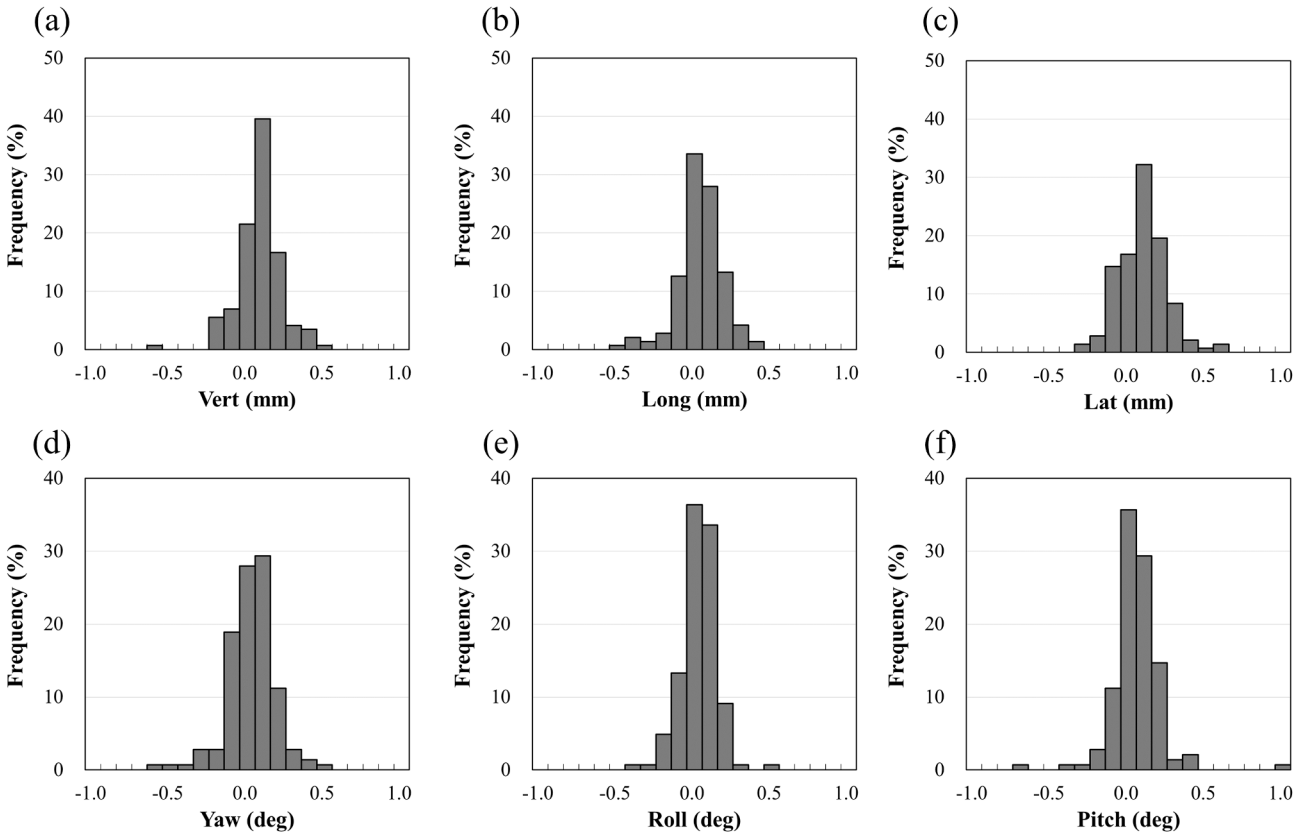

Fig. 5. Histograms of the deviations calculated immediately after the first X-ray verification in each direction. (a): vertical, (b) longitudinal, (c) lateral, (d) yaw, (e) roll, and (f) pitch.

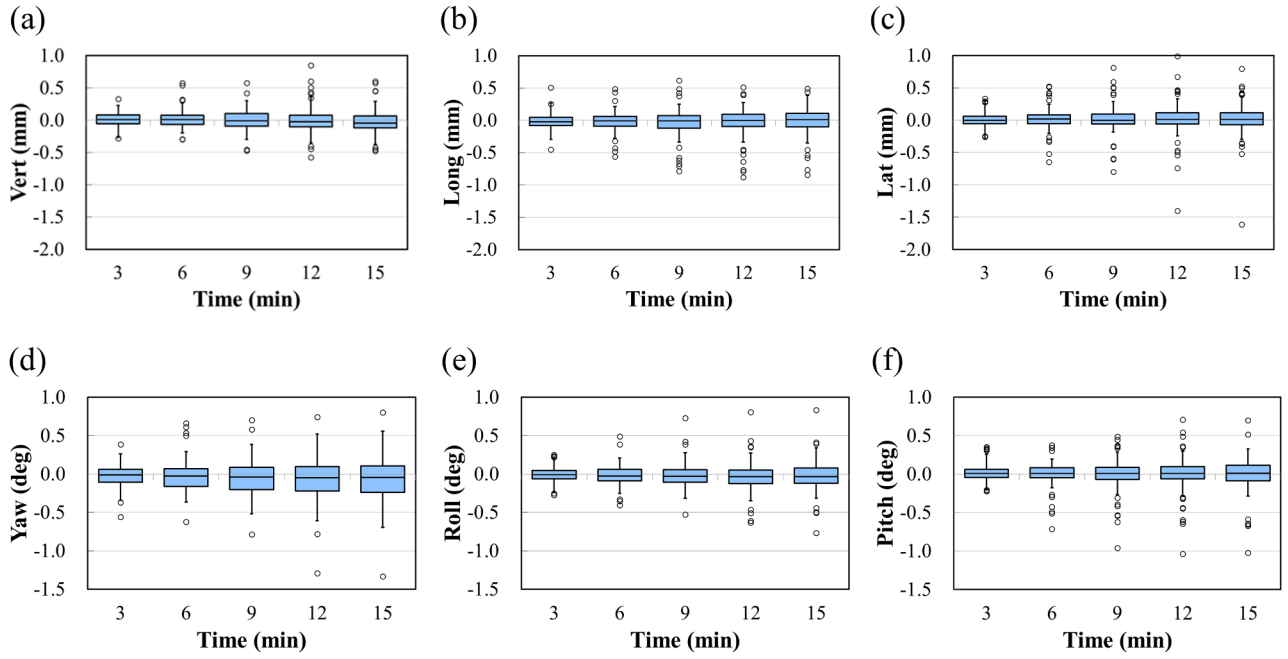

Fig. 6. Box-and-whisker plots of the variation of intrafractional motion (IFM) for translation (a, b, c) and rotation (d, e, f) during the examination period. The boxes represent the interquartile range (IR). Values below the first quartile minus 1.5 × IR are designated as low outliers, whereas those above the third quartile plus 1.5 × IR are designated as high outliers. From left to right, the data in graph represents IFM_2, IFM_3, IFM_4, IFM_5, and IFM_6 values, respectively.

in our study (i.e., a frameless mask, a 6-DOF robotic couch, and the ETX system). Ramakrishna et al. [10] found that the patient positioning of frame-based SRS using an X-ray image guidance system was highly accurate. Elsewhere, Li et al. reported on the patient positioning accuracy for invasive frame-based SRS using cone beam computed tomography. They reported translational and rotational errors of

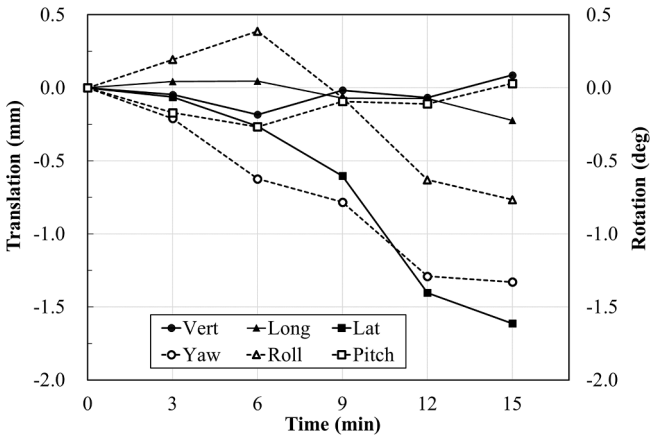

Fig. 7. Example of the trend of intrafractional motion for a patient whose intrafractional motion increased gradually during the examination period. The bite block was used for this patient.

0.08 ± 0.29 mm, -0.35 ± 0.50 mm, and -0.19 ± 0.32 mm for the vertical, longitudinal, and lateral axes, respectively, and $-0.03 \pm 0.19°$, $0.10 \pm 0.20°$, and $-0.14 \pm 0.25°$ for the yaw, roll, and pitch, respectively [23]. Our results were lower than those reported by Li et al. [23] and comparable with those reported by Verbakel et al. [11] and Keeling et al. [22] (Table 1), thereby demonstrating that the combination of frameless mask, 6-DOF robotic couch, and ETX can provide patient positioning with a comparable accuracy to frame-based techniques.

When comparing IFM performance with that reported in other studies, the immobilization device, treatment time, imaging device, and availability of a 6-DOF robotic couch are all factors that must be considered. Table 2 summarizes the patient motion from the pre- and post-treatment positions reported by other groups. The IFM evaluation method reported by Verbakel et al. [11] was similar to ours. They evaluated the IFM for an average of 16 min using an identical frameless mask and ETX system, recording results of -0.06 ± 0.19 mm, -0.01 ± 0.27 mm, and -0.04 ± 0.23 mm for the vertical, longitudinal, and lateral axes, respectively. Our results (IFM_6 and ${}^{3D}IFM_6$) were comparable with theirs, and those in our previous study [13]. Several groups reported IFM during irradiation for intracranial lesions [6,10,11,24]; however, it should be noted that they used different immobilization devices, examination durations, and imaging devices than those in our study.

Evaluating the values of *IP-IFM* is useful to confirm the patient position during treatment because the patients' head motion acquired from the pre- and post-treatment positions is not representative, as also found by Mangegius [12]. As shown in Fig. 9, a maximum value of 1.19 mm was suddenly observed for ${}^{long}IP\text{-}IFM_{3:2}$. Conversely, the value of ${}^{long}IFM_6$ was 0.13 mm. Using the values of *IFM* acquired from pre- and post-treatment verification, the target would not receive the planned dose

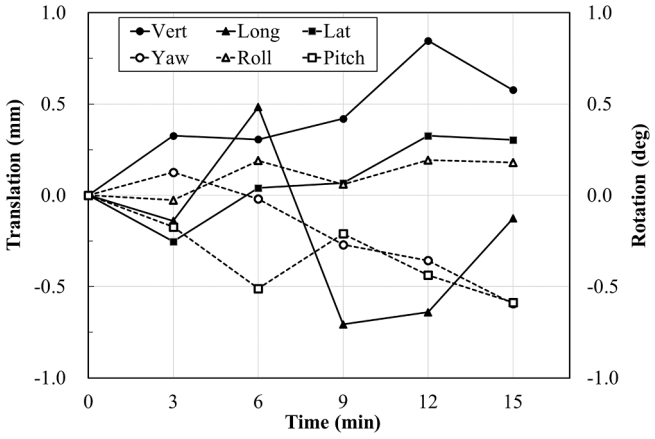

Fig. 9. Example of the trend of intrafractional motion for the patient who showed the largest inter-phase intrafractional motion (*IP-IFM*) value in this study. The bite block was used for this patient.

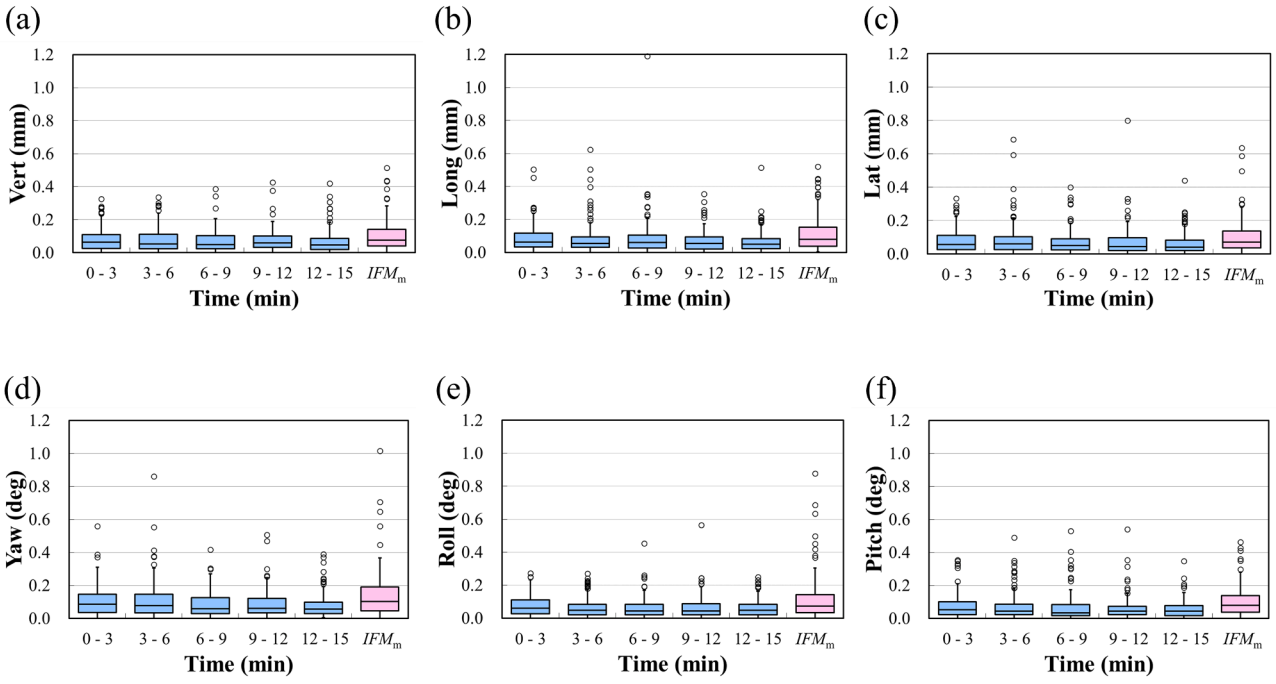

Fig. 8. Box-and-whisker plots of the variation of inter-phase intrafractional motion (*IP-IFM*) for translation (a, b, c) and rotation (d, e, f) during the examination period. From left to right, the data in each graph represents $IP\text{-}IFM_{2:1}$, $IP\text{-}IFM_{3:2}$, $IP\text{-}IFM_{4:3}$, $IP\text{-}IFM_{5:4}$, $IP\text{-}IFM_{6:5}$, and IFM_m values, respectively. The boxes represent the interquartile range (IR). Values below the first quartile minus 1.5 × IR are designated as low outliers, whereas those above the third quartile plus 1.5 × IR are designated as high outliers.

Table 1
List of positional deviations immediately after X-ray correction reported by other researchers and our group.

Authors	Number of fractions (Number of patients)	Positional deviation just after X-ray correction						Immobilization device	Imaging device
		Translation (mm)			Rotation (deg)				
		Vert	Long	Lat	Yaw	Roll	Pitch		
Li et al. [23]	17 (20)	0.08 ± 0.29	-0.35 ± 0.50	-0.19 ± 0.32	-0.03 ± 0.19	0.10 ± 0.20	-0.14 ± 0.25	No frameless mask	CBCT
Keeling et al. [22]	203 (35)	0.03 ± 0.21	-0.01 ± 0.26	-0.03 ± 0.25	-0.01 ± 0.24	0.00 ± 0.24	-0.03 ± 0.25	Frameless mask (not covered thin bone)	ETX
Vervakel et al. [11]	135 (46)	0.06 ± 0.26	0.04 ± 0.30	0.00 ± 0.24	0.03 ± 0.23	0.02 ± 0.15	0.01 ± 0.31	Frameless mask	ETX
Our study	143 (143)	0.03 ± 0.14	-0.03 ± 0.14	0.04 ± 0.15	-0.04 ± 0.15	-0.02 ± 0.11	0.00 ± 0.15	Frameless mask	ETX

The data are shown as mean ± standard deviation.
Abbreviations; ETX = ExacTrac X-ray system; CBCT = cone beam computed tomography.

Table 2
List of intrafractional motion reported by other researchers and our group.

Authors	Number of fractions (Number of patients)	Intrafractional motion (mm)				Definition of intrafractional motion (Examination duration)	Immobilization device	Imaging device
		Vert	Long	Lat	3D			
Ramakrishna et al. [10]	110 (7)	–	–	–	0.7 ± 0.5	Pre- and post-treatment (Not described)	Frameless mask (not covered mandible bone)	CBCT
Gevaert et al. [6]	66 (40)	–	–	–	0.58 ± 0.42	Pre- and post-treatment (14.6 min)	Frameless mask	ETX
Lewis et al. [24]	104 (104)	−0.10 ± 0.69	−0.06 ± 0.45	−0.08 ± 0.36	0.79 ± 0.45	pre- and during treatment (7.98 min)	Frameless mask (not covered mandible bone)	ETX
		0.05 ± 0.52	0.04 ± 0.39	−0.08 ± 0.35	0.65 ± 0.35	pre- and during treatment (4.87 min)		
Verbakel et al. [11]	79 (43)	−0.06 ± 0.19	−0.01 ± 0.27	−0.04 ± 0.23	0.35 ± 0.21	Pre- and post-treatment (16 min)	Frameless mask	ETX
Takakura et al. [13]	181 (181)	−0.05 ± 0.29	0.02 ± 0.42	−0.01 ± 0.49	–	Same as our study (21 min)	Frameless mask	ETX
Our study	143 (143)	−0.03 ± 0.12	−0.01 ± 0.20	0.03 ± 0.23	0.28 ± 0.21	IFM_6 (15 min)	Frameless mask	ETX
		0.11 ± 0.09	0.12 ± 0.11	0.10 ± 0.10	0.21 ± 0.14	IFM_m		

The data are shown as mean ± standard deviation (SD), but the data from Takakura et al. [14] are shown as mean ± 2SD.
Abbreviations: 3D = three-dimensional; IFM_6 = intrafractional motion defined as the deviation between the value calculated by ETX at phase-6 and that at phase-1; IFM_m = intrafractional motion defined as the deviation between the value calculated by ETX at the final X-ray verification and that at phase-6; ETX = ExacTrac X-ray system; CBCT = cone beam computed tomography.

because of the larger *IP-IFM* values. Noël et al. reported that a 1-mm margin of the gross tumor volume (GTV) for brain metastasis radiosurgery improved the probability of metastasis control without increasing side effects [25]. However, Nataf et al. reported that a 2-mm margin increased parenchymal complications [26]. Therefore, it is essential to maintain IFM within 1 mm during SRS. As the ceiling-floor-mounted device enabled us to periodically verify a patient's position without any mechanical movement of the X-ray tubes and flat panel detectors, the unexpected patient motion shown in Fig. 9 was successfully detected.

Although the IFM_m values for all patients were within 1 mm, the ${}^{lat}IFM_5$ and ${}^{lat}IFM_6$ values of the patient shown in Fig. 7, and the ${}^{long}IP\text{-}IFM_{3:2}$ value in Fig. 9 exceeded 1 mm. We did not understand the reasons for this outlying result. According to the statements on the electronic medical chart, the patient shown in Fig. 7 was extremely nervous at the pre-treatment examination, which could lead to increased movement. However, the nervousness of this patient was relieved by the experience of the pre-treatment examination. As a result, this patient underwent intracranial SRS without any problems. On the other hand, no unusual clinical and technical information about the patient in Fig. 9 was described in the pre-treatment examination.

To the best of our knowledge, this is the first detailed study to evaluate rotational IFM over time. The evaluation of rotational motion during treatment is particularly important in the case of single-isocenter VMAT for multiple brain metastases. For example, Roper et al. evaluated the dosimetric effects of rotational errors on target coverage single-isocenter VMAT for multiple brain metastases [16]. They suggested that rotational errors should be kept below 0.5° in light of the capabilities of real-time monitoring and the ability to correct couch rotation at each treatment center. Moreover, Prentou et al. simulated the dosimetric impact of rotational errors on target coverage and organs at risk, stating that rotational error should not exceed 0.5° [17]. Although Fig. 8 shows that the proportion of the rotational motion within 0.5° was more than 98.6% for all rotational directions in any *IP-IFM* values, rotational *IFM* values exceeding 0.5° were detected in a few patients. Therefore, we recommend periodic X-ray verification and correction for rotation as well as translation.

The original aim of this study was the evaluation of IFM_m values. In our study, the absence of a statistically significant relationship between ${}^{3D}IFM_6$ and ${}^{3D}IFM_m$ values suggests that the impact on patient position derived from elapsed time (i.e., 15 min) and that derived from a patient is equivalent. As mentioned above, with respect to the advantage of a 1-mm margin to the GTV for SRS, our results show that a frameless mask is capable of maintaining highly accurate positioning for performing single-isocenter SRS for multiple brain metastases. Nevertheless, a paradoxical problem exists between treatment time and positional error. Although X-ray verification and correction can improve patient positioning and reduce dosimetric deviation, these procedures may cause IFM owing to additional treatment time. This is supported by the study of Wang et al. [27], which reported that a consistent increase in the positioning deviation over time was observed. In contrast, Lewis et al. [24] investigated the necessity and frequency of monitoring IFM in

patients with frameless SRS. Based on their data, they concluded that imaging frequency could be reduced as there was no correlation between patient motion and treatment duration. However, verification and correction procedures for patient position should be decided carefully based on the ability to correct the 6D position and the feasibility of immediate X-ray verification as well as the patient immobilization device.

This study has several limitations because we have mainly focused on the patients' head motion during the actual treatment time. First, the mechanical accuracy was not evaluated. The required margins for SRS should be decided based on the overall accuracy of the gantry, couch, collimator rotation, and patient positioning. Second, we could not evaluate IFM at time intervals of X-ray verification shorter than 3 min. Different results may be acquired depending on the X-ray verification interval. Finally, we did not evaluate the effect of IFM on dose distributions. For single-isocenter VMAT for multiple brain metastases, the rotational error may have a more significant impact on the dose distributions of targets at a distance from the isocenter. Although other groups have already simulated the dosimetric effect of rotational deviation for intracranial SRS [15,16], further research on the dosimetric impact that considers both translational and rotational IFM is needed. Despite these limitations, our results may be useful for institutions that do not have imaging devices capable of verifying patient position rapidly and, therefore, might find frequent IFM evaluation difficult.

5. Conclusion

The $^{vert}IFM_p$ and $^{long}IFM_p$ values of all patients were within 1 mm irrespective of phase, with an error exceeding 1 mm observed in the $^{lat}IFM_5$ and $^{lat}IFM_6$ measurements for a single patient. The proportion of the rotational *IFM* values within 0.5° was more than 94.4% in any rotational direction. A movement exceeding 1 mm was observed in the $^{long}IP\text{-}IFM_{3:2}$ for one patient only. The proportion of *IP-IFM* values within 0.5° was more than 98.6% in any rotational direction. The translational IFM_m values were within 1 mm in all directions. The proportions of the rotational IFM_m values within 0.5° were 90.2%, 95.1%, and 93.0% for the yaw, roll, and pitch, respectively.

A frameless mask achieved highly accurate patient positioning and suppressed IFM by a combination of ETX and a 6-DOF robotic couch; however, a sudden large deviation was observed with low frequency. Therefore, X-ray verification and correction are required during treatment.

Acknowledgement

This work was supported in part by a JSPS Grant-in-Aid for Early-Career Scientists (Grant Number JP20K16723).

References

[1] Lightstone AW, Benedict SH, Bova FJ, Solberg TD, Stern RL. Intracranial stereotactic positioning systems: Report of the American Association of Physicists in Medicine Radiation Therapy Committee Task Group No. 68. Med Phys. 2005;32(7):2380-2398.
[2] Jin H, Keeling VP, Ali I, Ahmad S. Dosimetric effect of positioning shifts using 6D-frameless stereotactic Brainlab system in hypofractionated intracranial radiotherapy. J Appl Clin Med Phys 2016;17(1):102–11.
[3] Zhang M, Zhang Q, Gan H, Li S, Zhou S. Setup uncertainties in linear accelerator based stereotactic radiosurgery and a derivation of the corresponding setup margin for treatment planning. Phys Med 2016;32(2):379–85.
[4] Ackerly T, Lancaster CM, Geso M, Roxby KJ. Clinical accuracy of ExacTrac intracranial frameless stereotactic system. Med Phys 2011;38(9):5040–8.
[5] Gevaert T, Verellen D, Tournel K, Linthout N, Bral S, Engels B, et al. Setup accuracy of the novalis exactrac 6DOF system for frameless radiosurgery. Int J Radiat Oncol Biol Phys 2012;82(5):1627–35.
[6] Gevaert T, Verellen D, Engels B, Depuydt T, Heuninckx K, Tournel K, et al. clinical evaluation of a robotic 6-degree of freedom treatment couch for frameless radiosurgery. Int J Radiat Oncol Biol Phys 2011;83(1):467–74.
[7] Schmidhalter D, Fix MK, Wyss M, Schaer N, Munro P, Scheib S, Kunz P, Manser P. Evaluation of a new six degrees of freedom couch for radiation therapy. Med Phys 2013;40(11). 111710-1-11.
[8] BRAINLAB EXACTRAC Clinical User Guide, Revision 1.2. Available from: https://userguides.brainlab.com/wp-content/uploads/2020/01/ExacTrac-6.5-CUG-English-60919-86EN-Rev.1.2.pdf.
[9] EXACTRAC FRAMELESS RADIOSURGERY Clinical White Paper. Available from: https://www.brainlab.com/wp-content/uploads/2014/01/White-Paper-ExacTrac-Frameless-Radiosurgery.pdf.
[10] Ramakrishna N, Rosca F, Friesen Tezcanli E, Zygmanszki P, Hacker F. A clinical comparison of a patient setup and intra-fraction motion using frame-based radiosurgery versus a frameless image-guided radiosurgery system for intracranial lesions. Radiother Oncol 2010;95(1):109–1105.
[11] Verbakel W, Lagerwaard FJ, Verduin JE, Heukelom S, Slotman B, Cuijpers J. The accuracy of frameless stereotactic intracranial radiosurgery. Radiother Oncol 2010;97(3):390–4.
[12] Mangegius J, Seppi T, Weigel R, Arnold CR, Vasiljevic D, Goebel G, et al. Intrafractional 6D head movement increases with time of mask fixation during stereotactic intracranial RT-sessions. Radiat Oncol 2019;14(1):231.
[13] Takakura T, Mizowaki T, Nakamura M, Nakata M, Tsuruta Y, Miyabe Y, et al. Evaluation of intra-fractional motion in frameless stereotactic irradiation. Radiother Oncol 2012;103:S140.
[14] Kishi N, Nakamura N, Hirashima H, MukumotoN Takehana K, Uto M, Matsuo Y, et al. Validation of the clinical applicability of knowledge-based planning in single-isocenter volumetric modulated arc therapy for multiple brain metastasis. J Appl Clin Med Phys 2020;21(10):141–50.
[15] Sagawa T, Ohira S, Ueda Y, Akino Y, Mizuno H, Matsumoto M, et al. Dosimetric effect of rotational setup errors in stereotactic radiosurgery with HyperArc for single and multiple brain metastasis. J Appl Clin Med Phys 2019;20(10):84–91.
[16] Roper J, Chanyavanich V, Betzel G, Switchenko J, Dhabaan A. Single-isocenter multiple stereotactic radiosurgery: risk of compromised coverage. Int J Radiat Oncol Biol Phys 2015;93(3):540–6.
[17] Prentou G, Pappas E, Logothetis A, Koutsouveli E, Pantelis E, Papagiannis P, et al. Dosimetric impact of rotational errors on the quality of VMAT-SRS for multiple brain metastases: comparison between single- and two-isocenter treatment planning techniques. J Appl Clin Med Phys 2020;21(3):32–44.
[18] Gao J, Liu X. Off-isocenter Winston-Lutz test for stereotactic radiosurgery / stereotactic body radiotherapy. Int J Med Phys Clin Eng Radita Oncol 2016;5(2):154–61.
[19] Powell MJD. UOBYQA: unconstrained optimization by quadratic approximation. Math Program 2002;92(3):555–82.
[20] Hamada K, Fujibuchi T, Yoshida N, Ohura H. Examination of a dose evaluation method for floor-mounted kV X-ray image-guided radiation therapy systems. Radiol Phys Technol 2020;13:288–95.
[21] Implementation of the principle of as low as reasonably achievable (ALARA) for medical and dental personnel. NCRP Report 107. 1990.
[22] Keeling V, Hossain S, Jin H, Algan O, Ahmad S, Ali I. Quantitative evaluation of stereotactic radiotherapy with the frameless 6D ExacTrac system using statistical modeling. J Appl Clin Med Phys 2016;17(3):111–27.
[23] Li W, Cho YB, Ansell S, Ansell S, Laperriere N, Ménard C, et al. The use of cone beam computed tomography for image guided gamma knife stereotactic radiosurgery: initial clinical evaluation. Int J Radiat Oncol Biol Phys 2016;96(1):214–20.
[24] Lewis BC, Snyder WJ, Kim S, Kim T. Monitoring frequency of intra-fraction patient motion using the ExacTrac system for Linac-based SRS treatments. J Appl Clin Med Phys 2018;19(3):58–63.
[25] Noël G, Simon JM, Valery CA, Cornu P, Boisserie G, Hasboun D, et al. Radiosurgery for brain metastasis: impact of CTV on local control. Radiother Oncol 2003;68(1):15–21.
[26] Nataf F, Schlienger M, Liu Z, Foulquier JN, Grès B, Orthuon A, et al. Radiosurgery with or without a 2-mm margin for 93 single brain metastases. Int J Radiat Oncol Biol Phys 2008;70(3):766–72.
[27] Wang CW, Lin YC, Tseng HM, Xiao F, Chen CM, Cheng WL, Lu SH, Lan KH, Chen WY, Liang HK, Kuo SH. Prolonged treatment time deteriorates positioning accuracy for stereotactic radiosurgery. PLoS One 2015;10(4):1–10.

Physica Medica 98 (2022) 45–52

Contents lists available at ScienceDirect

Physica Medica

journal homepage: www.elsevier.com/locate/ejmp

Original paper

Evaluation of correlation between intrafractional residual setup errors and accumulation of delivered dose distributions in single isocenter volumetric modulated arc therapy for multiple brain metastases

Yusuke Tsuruta [a,b], Mitsuhiro Nakamura [b,c,*], Manabu Nakata [a], Hideaki Hirashima [c], Dejun Zhou [b], Megumi Uto [c], Keiichi Takehana [c], Takahiro Fujimoto [a], Takashi Mizowaki [c]

[a] Division of Clinical Radiology Service, Kyoto University Hospital, Kyoto 606-8507, Japan
[b] Division of Medical Physics, Department of Information Technology and Medical Engineering, Human Health Sciences, Graduate School of Medicine, Kyoto University, Kyoto 606-8507, Japan
[c] Department of Radiation Oncology and Image-applied Therapy, Graduate School of Medicine, Kyoto University, Kyoto 606-8507, Japan

ARTICLE INFO

Keywords:
Multiple brain metastases
Stereotactic radiotherapy
Residual setup error
Volumetric modulated arc therapy
Dose distribution

ABSTRACT

Purpose: To evaluate the displacement of gross tumor volume (GTV) positions caused by intrafractional residual setup errors (RSEs) and to accumulate delivered dose distributions considering intrafraction RSEs in fractionated-stereotactic radiotherapy (f-SRT) with single isocenter volumetric modulated arc therapy (SI-VMAT) for multiple brain metastases.

Methods: Overall, 72 consecutive patients who underwent f-SRT with SI-VMAT for multiple brain metastases were included. For all patients, 6D correction was performed using the ExacTrac X-ray (ETX) system. GTV displacement (ΔD) was calculated considering the intrafractional RSEs measured by the ETX system during irradiation. The correlation between ΔD and the distance from the isocenter to each GTV (d) was analyzed. Computed tomography (CT) images considering the intrafractional RSEs were generated for five patients with $\Delta D > 1$ mm. The delivered dose distributions for all fractions were reconstructed on the corresponding CT, followed by their accumulation.

Results: The 95th percentile of ΔD from 7,270 resultant center positions of 417 GTVs was 0.92 mm. No correlation was observed between ΔD and d. For 53 GTVs from five patients with $\Delta D > 1$ mm, the difference of GTV $D_{99.5\%}$ and $D_{0.5\%}$ between the planned and accumulated values was $-0.4 \pm 2.5\%$ and $-1.0 \pm 0.8\%$, respectively. There was no correlation between d and the difference of GTV $D_{99.5\%}$ and $D_{0.5\%}$.

Conclusions: We found no significant difference in GTV $D_{99.5\%}$ and $D_{0.5\%}$, despite the location of GTVs far from the isocenter. However, it should be noted that this result was because the intrafractional RSEs were reduced to a clinically acceptable level.

Introduction

Brain metastases occur in 20–40% of cancers and are the most common intracranial tumors [1]. Radiotherapy (whole brain radiotherapy [WBRT], fractionated stereotactic radiotherapy [f-SRT], and stereotactic radiosurgery [SRS]) is widely used to treat brain metastases. Conventionally, WBRT is performed for most patients with brain metastases to control the local tumor and prevent neurological death [2]. Recently, researchers have increasingly shifted their attention to f-SRT and SRS owing to WBRT-mediated deterioration of neurocognitive function and the quality of life [3,4].

Linear accelerator (Linac)-based f-SRT and SRS conventionally requires a setting of individual isocenter for each target. These techniques lengthen the treatment time for patients with multiple brain metastases. Patient movement increases during irradiation with prolonged treatment time [5], thereby necessitating accurate irradiation in the shortest possible duration. Single isocenter volumetric modulated arc therapy (SI-VMAT) has recently been identified as an attractive technique that can overcome the aforementioned problem. This technique can irradiate multiple brain metastases simultaneously at a single isocenter.

* Corresponding author at: Division of Medical Physics, Department of Information Technology and Medical Engineering, Human Health Sciences, Graduate School of Medicine, Kyoto University Kyoto 606-8507, Japan.
E-mail address: m_nkmr@kuhp.kyoto-u.ac.jp (M. Nakamura).

https://doi.org/10.1016/j.ejmp.2022.04.012
Received 2 December 2021; Received in revised form 30 March 2022; Accepted 22 April 2022
Available online 28 April 2022

Intracranial stereotactic irradiation (STI) with SI-VMAT is reportedly more efficient in terms of monitor units (MUs), treatment time, and conformity than SRS with multiple isocenters [6–8].

One of the most important aspects of radiotherapy is how accurately any process is executed as per the treatment plan. However, there are some patient- or treatment machine-derived uncertainties in the course of radiotherapy. These uncertainties should be as few as possible, especially in STI with SI-VMAT. Recently, it has become possible to confirm patient position at any time due to the development of image-guided devices [9]. As a result, the accuracy of patient positioning has increased in STI [10]. The 6D correction using the ExacTrac X-ray (ETX) system has also contributed to highly accurate [11] and time-efficient positioning [12,13].

Despite shortening the treatment time, however, slight residual setup error (RSE) persists during irradiation [14]. In particular, the rotational components of RSEs lead to localization errors for targets located far from the isocenter in STI with SI-VMAT for multiple brain metastases. Several groups have simulated the effects of pseudo rotational errors on dose distribution [15,16]. They intentionally generated uniform rotational error with 0.5°, 1.0°, and 2.0° around every orthogonal axes and suggested that the rotational error should be $\leq$0.5° considering that the dose coverage to targets are dependent on the distance between a target and the treatment isocenter. However, they did not examine the effect of translational error on dose distribution. Contrastingly, some researchers have reported on the importance of repeatedly verifying and rectifying the patient position because intrafractional RSEs occur suddenly and cannot be completely suppressed during irradiation [14,17]. In STI with SI-VMAT for multiple brain metastases, target sizes and treatment margins are generally small. Additionally, the distance between a target and treatment isocenter varies; therefore, it is crucial to understand the effect of the intrafractional RSEs in translation and rotation on dose distributions.

This study aimed to evaluate the displacement of target positions caused by intrafractional RSEs acquired during STI with SI-VMAT using the ETX system for 6D correction, and to accumulate delivered dose distributions using generated computed tomography (CT) images considering the intrafractional RSEs.

Material and methods

Patient characteristics and treatment planning

This study was conducted in accordance with the Declaration of Helsinki. Overall, 72 consecutive patients who underwent f-SRT with SI-VMAT technique for multiple brain metastases between April 2017 and June 2019 were included in this study. With the approval of the institutional review board (approval number: R1167), written informed consent was obtained for all patients. All patients were immobilized with a frameless mask of type B R408 (Klarity Medical & Equipment Co., Ltd., Guangzhou, China). Planning CT images were acquired using a SOMATOM Definition AS instrument (Siemens, Erlangen, Germany). CT images were reconstructed using a slice thickness of 1.0 mm and exported to the Eclipse (Varian Medical Systems, Palo Alto, CA). Furthermore, gadolinium-enhanced T1-weighted magnetic resonance (MR) images obtained within 1 month prior to CT simulation were combined with CT images in the Eclipse. Our treatment plan followed the method proposed by Kishi et al. [18]. Gross tumor volumes (GTVs) were defined as visible lesions on the CT and MR images. Planning target volumes (PTVs) were generated by adding 1 mm margin to GTVs. A total of three to five arcs (one or two coplanar arcs and two or four non-coplanar arcs) were used. The treatment isocenter was located at a position with approximately equal distances from each GTV. All VMAT plans were created with arcs for 10 MV-FFF X-ray. The dose to 99.5% of the PTVs (PTV $D_{99.5\%}$ = 100%) was prescribed for each plan. Plan optimization was performed such that the maximum dose to all PTVs was approximately 135–150%. Dose calculations were performed using Acuros XB (ver. 15.6; Varian Medical Systems, Palo Alto, CA), with heterogeneity correction and a 1-mm grid resolution. Table 1 summarizes the patient characteristics and treatment plan.

Irradiation procedure

TrueBeamSTx (Varian Medical Systems, Palo Alto, CA) was used for irradtiation. Isocenter localization accuracy was daily evaluated using Winston-Lutz (WL) test. After the phantom setup was completed, the MV images were acquired at gantry angles of 0°, 90°, 180°, and 270° using electronic portal imaging device with TrueBeam. The pixel size was 0.22 mm at the isocenter [19]. In our institution, the laser alignment was maintained so that the results of the WL test was within 0.5 mm in each direction. The images were analysed using the TM-WINS (R-TECH.INC, Tokyo, Japan). The ETX system and a six-degrees-of-freedom couch (Brainlab, Feldkirchen, Germany) were used for patient positioning. The pixel size of the flat panel detector was 0.26 mm at the isocenter [20]. Before clinical use, the ETX system was well-commissioned in the phantom experiment, and a total of 90 tests were conducted. The accuracy of the correction for known values (translation and rotation) was evaluated.

Following the infrared reflective-based positioning, a pair of kV X-ray images were acquired and automatically matched with digitally reconstructed radiographs. The ETX-calculated values were applied to correct the patient position in translation and rotation (X-ray correction). X-ray correction was performed until reaching values within the institutional tolerance ones as determined from our phantom study in the commissioning process (0.7 mm/1.5°). Values within the tolerance were recorded as intrafractional RSEs. After irradiating the first arc (coplanar beam: couch angle was 0°), the couch was rotated for the second arc. Subsequently, a pair of X-ray images were captured for verifying the patient position. X-ray verification and X-ray correction (if needed) were repeatedly performed until the values were within tolerance. This procedure was repeated on rotating the treatment couch each time.

Displacement of GTV positions caused by intrafractional RSEs

The planned center position of a GTV from the isocenter was defined as (X, Y, and Z), where X, Y, and Z denote lateral, vertical, and longitudinal directions, respectively. These values were calculated using the Eclipse. The distance between the planned center position of each GTV and the isocenter (d) was calculated from the square root of the sum of squares of X, Y, and Z. With (x, y, z) in translation and (α, β, γ) in rotation as intrafractional RSEs, the resultant center position of a GTV (^{r}X, ^{r}Y, ^{r}Z)

Table 1
Patient characteristics.

Number of patients (male/female)	72 (32/40)
Age (y)	64.5 (29–88)
Tumor volume (cm^3)	0.15 (0.01–27.02)
Distance between GTV and isocenter (mm)	48.5 (4.9–95.0)
Number of GTVs per patient	5 (2–19)
Beam arrangement	
3 arcs (1 coplanar arc and 2 non-coplanar arcs)	69
5 arcs (1 coplanar arc and 4 non-coplanar arcs)	3
Prescribed dose (total dose/number of fractions)*	
38 Gy/10fr	4
20 Gy/5fr	2
28 Gy/5fr	65
30 Gy/5fr	1

Data are shown in median (minimum–maximum).
*The maximum dose to all PTVs was around 135–150%.
Abbreviation: GTV = gross tumor volume.

was calculated by the following equation:

$$\begin{pmatrix} {}^{r}X \\ {}^{r}Y \\ {}^{r}Z \end{pmatrix} = \begin{pmatrix} \cos\gamma & -\sin\gamma & 0 \\ \sin\gamma & \cos\gamma & 0 \\ 0 & 0 & 1 \end{pmatrix} \begin{pmatrix} \cos\beta & 0 & -\sin\beta \\ 0 & 1 & 0 \\ \sin\beta & 0 & \cos\beta \end{pmatrix} \begin{pmatrix} 1 & 0 & 0 \\ 0 & \cos\alpha & \sin\alpha \\ 0 & \sin\alpha & -\cos\alpha \end{pmatrix} \begin{pmatrix} X \\ Y \\ Z \end{pmatrix} + \begin{pmatrix} x \\ y \\ z \end{pmatrix} \quad (1)$$

Eventually, the distance between the planned and resultant center positions of each GTV (ΔD) was calculated by the following equation:

$$\Delta D = \sqrt{\left({}^{r}X - X\right)^2 + \left({}^{r}Y - Y\right)^2 + \left({}^{r}Z - Z\right)^2} \quad (2)$$

The in-house program edited with Python script (Python version 3.9.2) was used for calculating ΔD. Pearson's correlation between ΔD and d was analyzed.

Accumulating dose distributions on generated CT images considering intrafractional RSEs

Of the 72 patients, five patients who had more than five GTVs, and GTVs with $\Delta D > 1$ mm just before irradiation in each arc were selected. These patients received five fractionated treatment plans with three arcs (one coplanar arc and two non-coplanar arcs) per fraction. The frequency of $\Delta D > 1$ mm from the five patients are summarized in Table 2. Seventy-five CT images were generated, considering the intrafractional RSEs for each arc (15 CT images per patient = three arcs × five fractions) using an in-house Python script (ver. 3.9.2). CT images, including the intrafractional RSEs, were defined as "generated CT." After the Digital Imaging and Communications in Medicine files of CT volume were input, the program first calculated the center position of each voxel. Then, the program calculated the rotated position of each voxel based on the treatment isocenter (X, Y, Z) and rotation degree (α, β, γ) in each axis, thus generating the rotated CT volume. The rotated CT images were resampled from the rotated CT volume with the same position of origin CT images. Linear interpolation was adapted during the resampling. Finally, whole voxels were shifted based on the corresponding translation (x, y, z) in each axis. All generated CT images for each patient were imported to the Eclipse. The delivered dose distribution for each arc of each fraction was reconstructed on each generated CT image while maintaining the same MUs and leaf motion with the original plan. Thereafter, each dose distribution was automatically accumulated based on spatial information in 3D space between the original and generated CT to obtain one for the sum of five fractions (accumulated dose distribution). The $D_{99.5\%}$, $D_{98\%}$, and $D_{0.5\%}$ of GTV acquired from the accumulated dose distributions were compared with those obtained from planned dose distributions. Additionally, a biologically effective dose with α/β of 12 Gy for GTV $D_{98\%}$ (GTV $BED_{12\ 98\%}$) was calculated.

Table 2
The proportions (frequency) of $\Delta D > 1$ mm for five patients.

Patients' number	Number of GTVs	Percentages (frequency) of $\Delta D > 1$ mm (%)*
8	18	5.6 (15/270)
37	15	8.9 (20/225)
50	6	7.8 (7/90)
60	8	7.5 (7/120)
65	6	15.6 (14/90)

* The denominator is the product of the number of GTVs, the number of fractions (5 fractions) and the number of arcs (3 arcs).
Abbreviations: GTV = gross tumor volume; ΔD = displacement of GTV caused by the intrafractional residual setup errors.

After testing whether these dose volume indices were normally distributed using the Shapiro–Wilk test, statistical analysis was performed between planned and accumulated dose distributions. The paired t-test was used for data with a normal distribution, and Mann–Whitney U test for data lacking a normal distribution, at a significance level of 5%. Pearson's correlation between each dose volume index and d or GTV size was calculated. Fig. 1 depicts a workflow of this study.

Results

The results of the WL test performed from April 2017 to June 2019 and the commissioning test for the ETX system are shown in Table 3.

The mean ± standard deviation (SD) of all 1,180 intrafractional RSEs were 0.1 ± 0.2 mm, 0.0 ± 0.2 mm, 0.1 ± 0.3 mm in the vertical, longitudinal, and lateral direction and 0.0 ± 0.2°, 0.1 ± 0.2°, 0.1 ± 0.2° in the pitch, yaw, and roll axes, respectively. The percentage (frequency) of the rotational RSE over 0.5° on two axes was only 0.7% (9/1,180). No patient was observed to have >1.0° degree of intrafractional RSEs on multiple axes. Fig. 2 summarizes intrafractional RSEs in all directions and axes.

A total of 7,270 resultant center positions from 417 GTVs with intrafractional RSEs were analyzed. All of the intrafractional RSEs were kept within our institutional torelance (0.7 mm/1.5°). The maximum ΔD was 1.9 mm at a GTV with d of 73.3 mm. Fig. 3(a) depicts the correlation between ΔD and d. No correlation was observed between ΔD and d (r = 0.11). Fig. 3(b) depicts the frequency distribution and cumulative histogram of ΔD. The frequency of $\Delta D < 1$ mm was 97.0%. The 95th percentile of ΔD was 0.92 mm.

Figure 4 depicts the correlation between the planned and accumulated dose volume indices for GTVs from the five patients. The mean ± SD of the difference of GTV $D_{99.5\%}$, $D_{98\%}$, and $D_{0.5\%}$ between the planned and accumulated values were −0.4 ± 2.5%, −0.9 ± 2.9%, and −1.0 ± 0.8%, respectively. The planned and accumulated GTV $BED_{12\ 98\%}$ were 54.6 ± 3.5 Gy and 54.1 ± 4.0 Gy, respectively. For 33 of 53 GTVs, GTV $BED_{12\ 98\%}$ in the accumulated dose distribution were higher than 52.4 Gy. No significant difference was observed between the planned and accumulated dose distributions (GTV $D_{99.5\%}$, $p = 0.47$; $D_{98\%}$, $p = 0.25$; and $D_{0.5\%}$, $p = 0.16$; GTV $BED_{12\ 98\%}$, $p = 0.25$).

Figure 5 depicts the effect of ΔD, d, and GTV size on differences in dose volume indices. There were no correlations between ΔD and the difference of GTV $D_{99.5\%}$ ($r = -0.01$), $D_{98\%}$ ($r = -0.01$), and $D_{0.5\%}$ (r = 0.03) for each arc of each fraction [Fig. 5(a)]. Differences of $D_{99.5\%}$ and $D_{98\%}$ between the planned and accumulated values were within ±5% for 48 of 53 GTVs [Fig. 5(b) and (c)]. For all GTVs of five patients, differences of $D_{0.5\%}$ between the planned and accumulated values were within ±3.1%. For 53 GTVs from the five patients, there was no correlation between d and the difference of GTV $D_{99.5\%}$ ($r = -0.04$), $D_{98\%}$ ($r = 0.19$), and $D_{0.5\%}$ ($r = -0.17$) [Fig. 5(b)]. Moreover, there was no correlation between GTV size and the difference of dose volume indices, GTV $D_{99.5\%}$ ($r = -0.09$), $D_{98\%}$ ($r = 0.05$), and $D_{0.5\%}$ ($r = 0.30$) [Fig. 5(c)].

Figure 6 depicts an overview of a GTV in original plan and accumulated plan. The largest difference in $D_{98\%}$ were observed in this case. A yellow and red circle denotes the contour of a GTV and the 110% isodose line, respectively. The accumulated $D_{98\%}$ was 110.3%, and the difference of $D_{99.5\%}$ from the planned value was −9.2%.

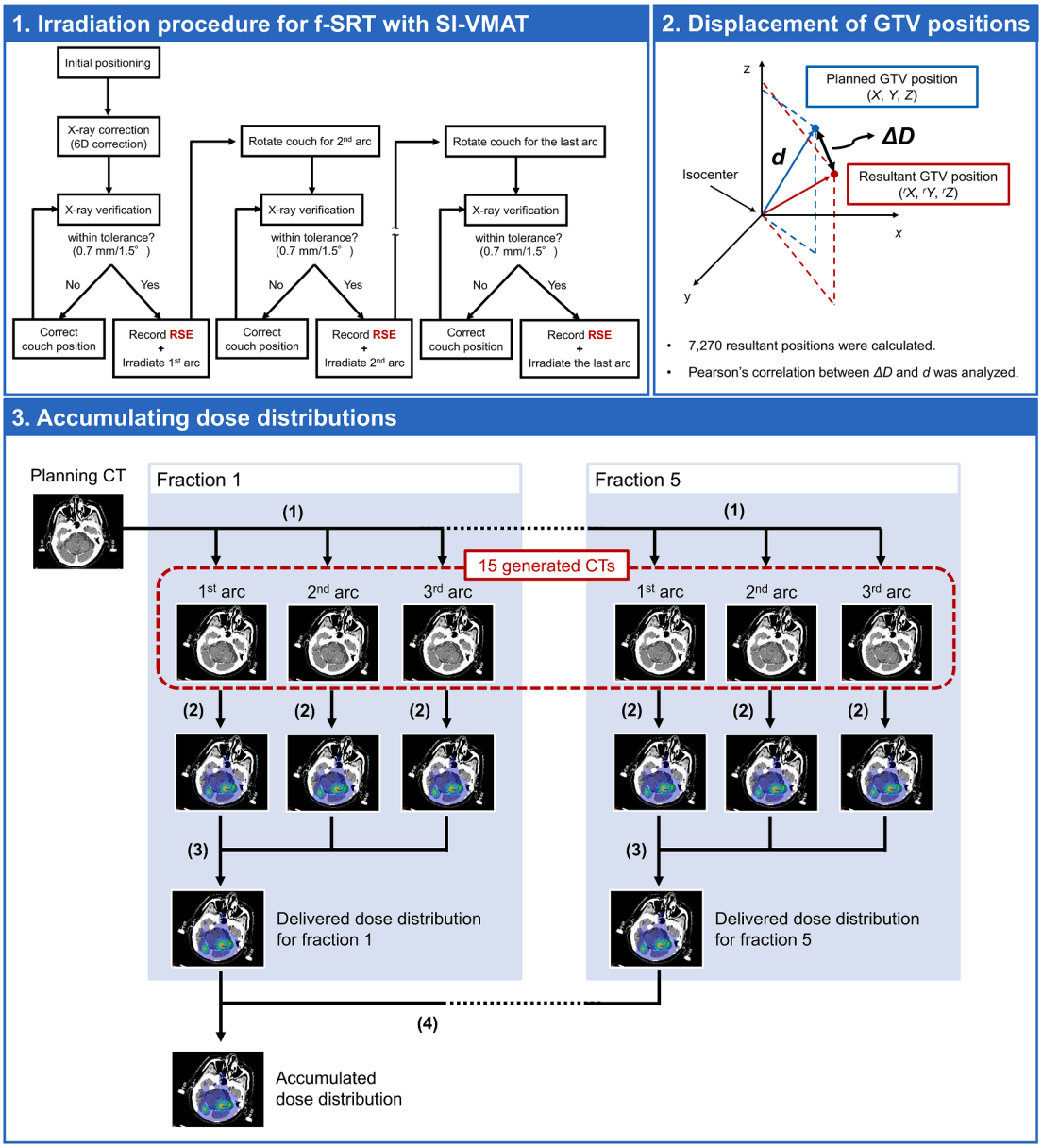

Fig. 1. Study workflow. To accumulate the dose distributions four processes were required. (1) Fifteen CT images per patient were generated using an in-house Python script. Intrafractional RSEs were included in the generated CT images. (2) The delivered dose distribution for each arc was reconstructed on each generated CT. (3) The delivered dose distribution for each fraction was acquired as the sum of that for each arc. (4) The accumulated dose distribution was acquired as the sum of the dose distributions for the five fractions. Abbreviations: *d*, distance between GTV position and treatment isocenter; $D_{xx\%}$, dose to xx% of GTV; f-SRT, fractionated stereotactic radiotherapy; *ΔD*, displacement of GTV caused by the intrafractional residual setup errors; RSE, residual setup error; GTV, gross tumor volume; SI-VMAT, single isocenter volumetric modulated arc therapy; CT, computed tomography.

Table 3
Results of the WL test and commissioning test of the ETX.

	Vert (mm)	Long (mm)	Lat (mm)	Yaw (deg)	Roll (deg)	Pitch (deg)
WL	0.1 ± 0.3	0.0 ± 0.3	0.0 ± 0.5	–	–	–
ETX	0.0 ± 0.1	0.0 ± 0.1	0.0 ± 0.0	0.0 ± 0.1	−0.1 ± 0.1	−0.1 ± 0.1

The data are shown as mean ± 2SD.
Abbreviation: Vert = vertical; Long = longtitudinal; Lat = lateral; WL = Winston-Lutz test; ETX = ExacTrac X-ray.

Discussion

This study analyzed the displacement of GTV position and the effect of intrafractional RSEs on the dose distribution. In the simulation study conducted by Rojas-López et al., the positional deviation of >1 mm was observed for targets of >50 mm away from the isocenter when 0.5° of rotation was generated in all three axes [21]. In our study, the percentage of the rotational RSE over 0.5° on two axes was only 0.7%. Accordingly, the displacement of each GTV in our study would be considered to be equal to or less than their results. To analyze the delivered dose distribution for targets, actual positional errors are required, particularly ones located away from the isocenter. Previously published reports identified the distance from the isocenter to the target as one of the most important factors in the accurate irradiation of STI with SI-VMAT for multiple brain metastases [15,16,21–23]. In contrast

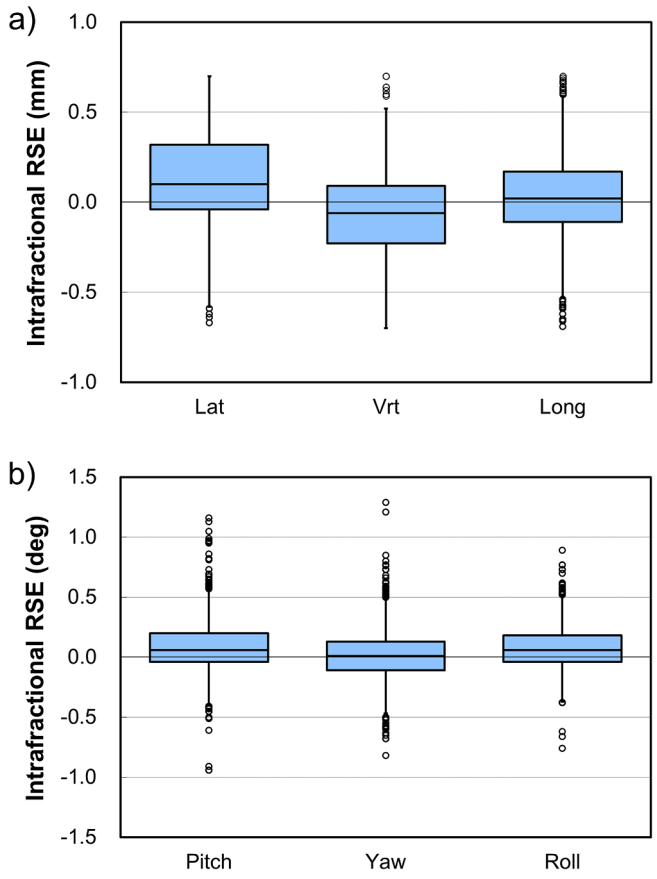

Fig. 2. Box-and-whisker plots of the intrafractional RSEs for translation (a) and rotation (b). Boxes represent the interquartile range (IR). Values below the first quartile minus 1.5 × IR are designated as low outliers, whereas those above the third quartile plus 1.5 × IR are designated as high outliers.

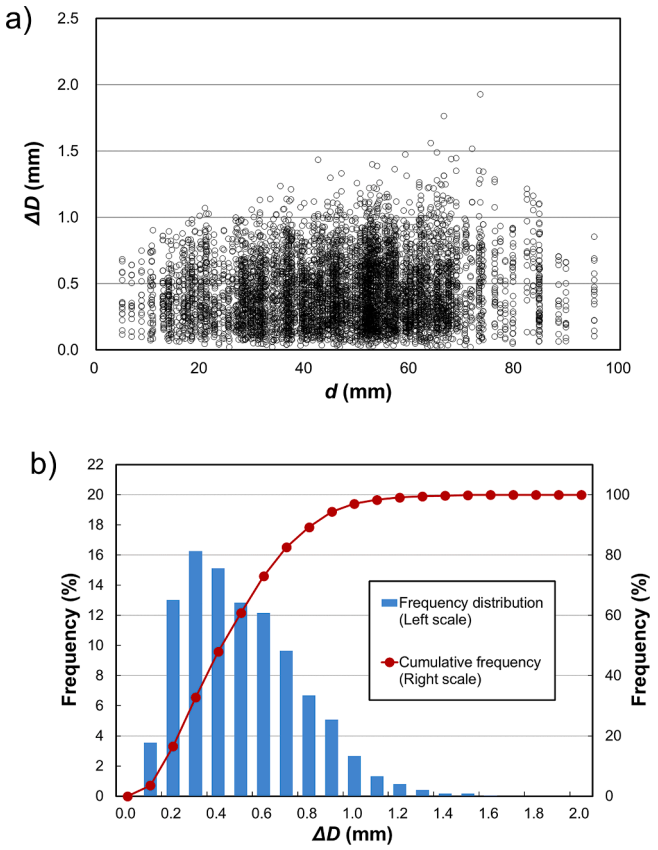

Fig. 3. (a) Correlation between ΔD and d. (b) Frequency distribution and cumulative histogram of ΔD. The frequency of $\Delta D < 1$ mm was 97.0%. The 95th percentile of ΔD was 0.92 mm. Abbreviations are as in Fig. 1.

to these studies, there was no correlation between d and ΔD ($r = 0.11$) until the intrafractional RSEs were kept within the tolerance (0.7 mm/1.5°). Recently, Tsuruta et al. have demonstrated that the maximum value of intrafractional patient head motion at 3-min intervals was 1.19 mm and 0.89° using a frameless mask and six-degrees-of-freedom robotic couch and suggested that verification and correction of patient position be periodically performed [17]. Taken together, it is important to maintain intrafractional RSEs at the lowest possible values while irradiating GTVs located far from the isocenter in STI with SI-VMAT.

The analysis of dose distribution is essential for GTVs with larger displacement than the margin. To the best of our knowledge, this is the first report on the accumulated dose distribution, considering the intrafractional RSEs. For 53 GTVs from five patients, there was no correlation between dose volume indices and d or GTV size. Additionally, there was no significant difference between the planned and accumulated dose distributions. In terms of the correlation between d and dose volume indices, Kraft et al. reported that STI with SI-VMAT for multiple brain metastases achieved high local control rates regardless of the distance to the isocenter [24]. Our data supported the results from Kraft et al. in terms of dose distribution for STI with SI-VMAT. Dupic et al. reported on GTV $D_{98\%}$ as a significant predictor for local control. GTV $D_{98\%}$ >29.4 Gy in three fractions, which is equivalent to GTV $BED_{12\ 98\%}$ >52.4 Gy, significantly improved the local control of patients aged ≥18 years who underwent STI with SI-VMAT for tumors >2 cm in diameter [25]. In our study, however, our protocol was different from the aforementioned studies in terms of dose prescription, fractionation, and tumor size (Table 1). Hence, we have analyzed the clinical outcomes based on GTV $BED_{12\ 98\%}$, with reference to the results of Dupic et al. In contrast, in terms of the correlation between target size and dose volume indices, our results differed from those of previous studies [26,27]. This is mainly due to the fact that we focused on GTVs, rather than PTVs. Minniti et al. reported that PTV size was one factor associated with PTV dose coverage [26]. However, they added a 1 or 2 mm margin for PTV, and the PTVs received at least 98% of the prescribed dose. In general, GTV delineation is always performed in the same way; however, PTV margins differ between institutions. Thus, when making comparisons with previous studies, it is important to clarify the main target volume of analysis.

The required PTV margin should be set carefully in STI with SI-VMAT for brain metastases. Nakano et al. performed geometrical simulation depending on the target size and the distance from the isocenter to a target to clarify the required PTV margin for target coverage [22]. The margin might have to be larger with a smaller target size and longer distance from the isocenter. In contrast, Nataf et al. reported that the PTV margin of 2 mm could cause a significantly high incidence of serious complications with margin expansion [28]. Kirkpatrick et al. reported that a PTV margin of 1 mm may be more appropriate for an intracranial tumor with SRS because of the higher risk of radionecrosis [29]. In this study, PTV margins of 1 mm were added to GTV. Fig. 6 shows that GTV coverage was reduced in the accumulated plans because the GTV position was deviated from the center of planned dose distribution. However, we believe that the PTV margin is appropriate because no significant difference was observed between the planned dose distributions and the accumulated ones.

Our data were also important in terms of the post-treatment quality assurance (QA). While researchers have established guidelines and methodologies for pre-treatment QA, as represented by the Reports from American Association of Physicists in Medicine task group [30–32], there is no established method for post-treatment QA. Quantifying the actual delivered dose to patients using the acquired during irradiation is

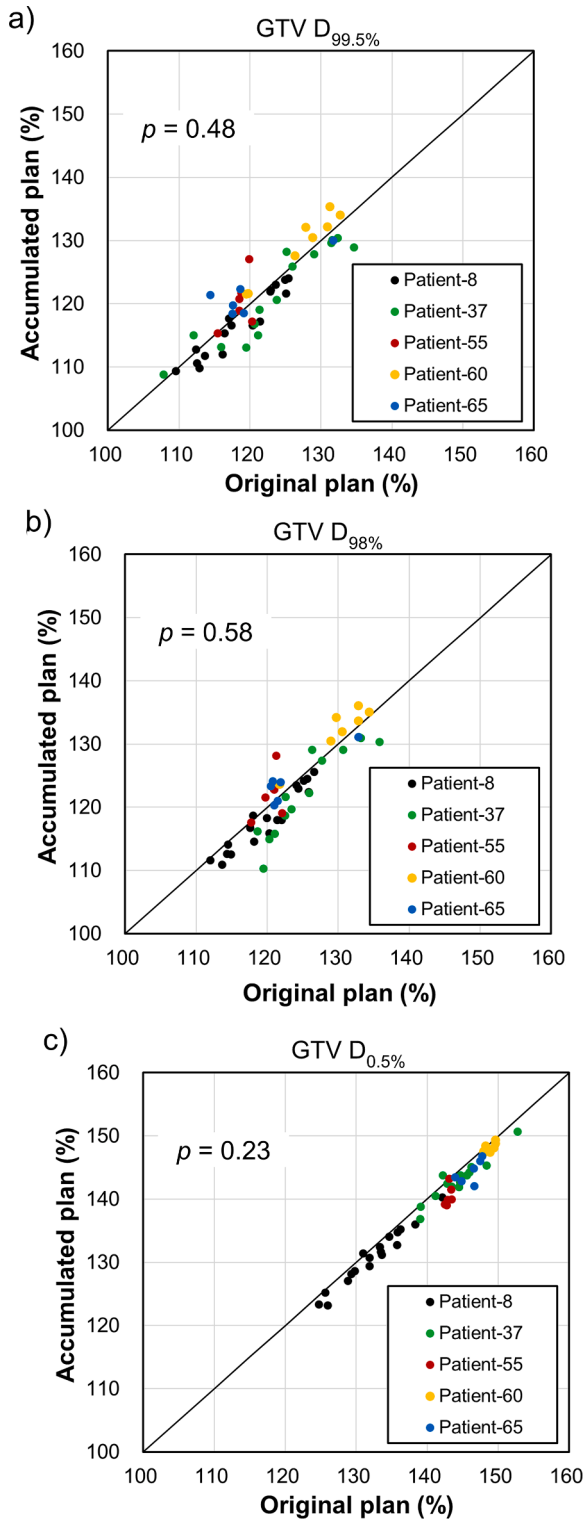

Fig. 4. Correlations between the planned and accumulated dose volume indices for GTVs. (a) GTV $D_{99.5\%}$, (b) GTV $D_{98.0\%}$, and (c) GTV $D_{0.5\%}$. Abbreviations are as in Fig. 1.

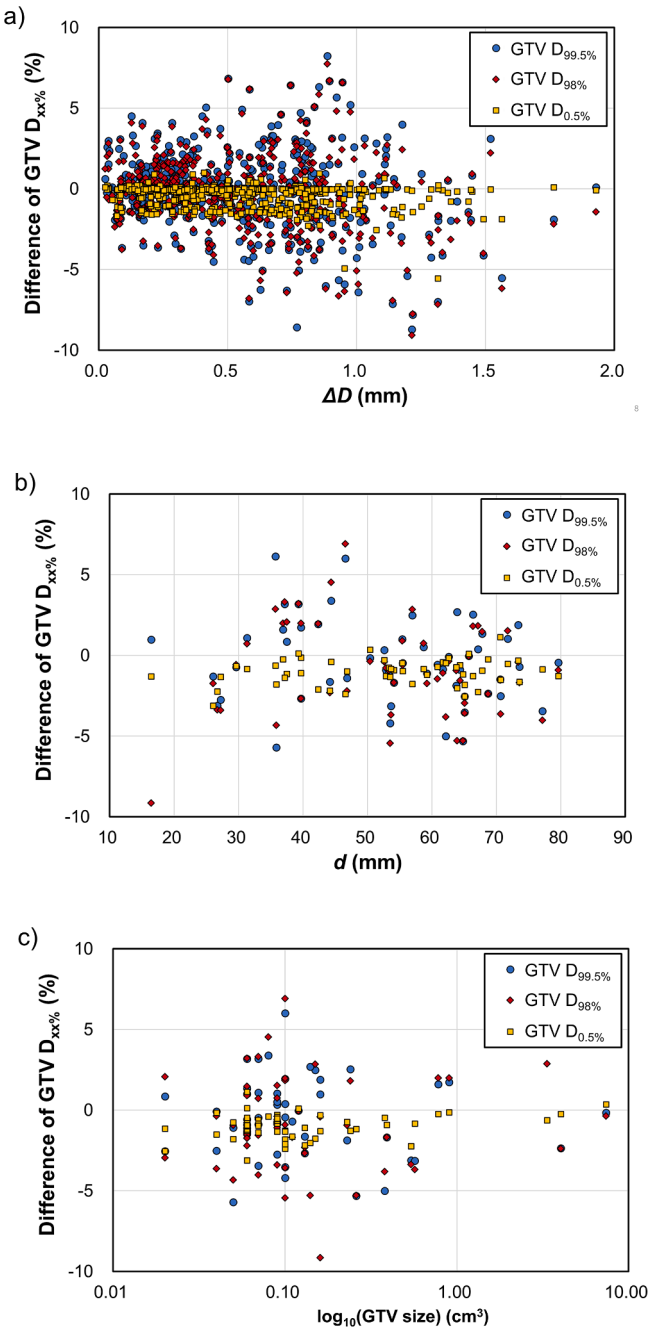

Fig. 5. Differences between the delivered and planned dose volume indices for GTV for each arc of each fraction as a function of ΔD (a). Differences between the accumulated and planned dose volume indices for GTVs as a function of d (b), and GTV size (c). Abbreviations are as in Fig. 1.

a challenge for improving the accuracy of radiotherapy. In vivo dosimetry is used for estimating the delivered dose to a patient through a direct measurement of the treatment beam [33,34] and plays an important role in improving the accuracy of radiotherapy. Ideally, dosimeters would be implanted in the patient's body to measure the delivered dose during irradiation; however, it is not practical for the intracranial region because of invasiveness. The use of data acquired or generated during treatment is another method to reconstruct the delivered dose distribution. The method presented in this study enabled the accumulation of the delivered dose distribution based on the generated CT images with intrafractional RSEs. In contrast, delivered information such as the multi-leaf collimator position, gantry angle, and delivered MU at each control point were also available from the log file. Several research groups have reported on dose reconstruction considering mechanical position errors by log files [35,36]. The log file-based analysis obtained during irradiation demonstrated that the geometric accuracy of the linac was highly accurate. Our study principally focused on patient positioning errors because the effect of intrafractional RSEs

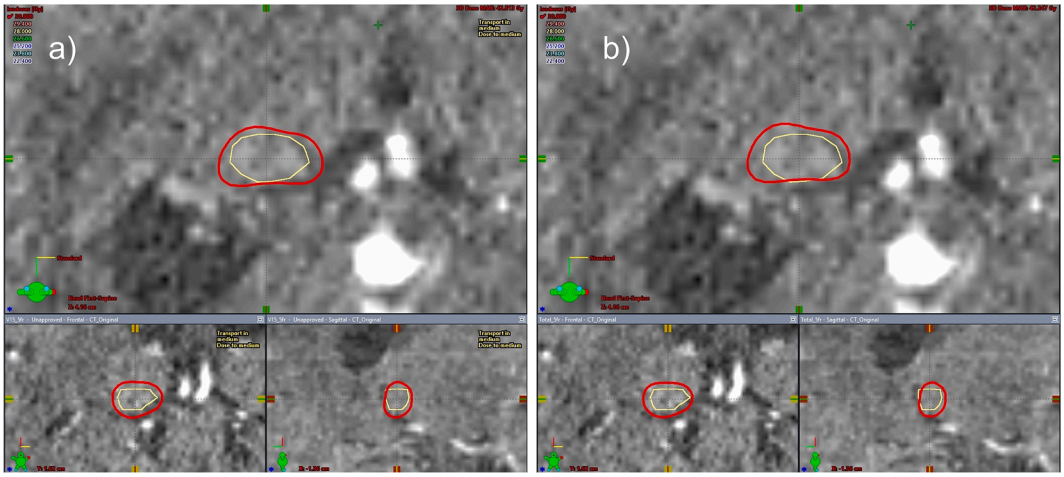

Fig. 6. Overview of a GTV in the original plan (a), and accumulated plan (b). A yellow circle denotes the contour of a GTV with a volume of 0.16 cm^3, and a *d* of 16.4 mm. A red circle denotes 110% isodose line. The $D_{98\%}$ was 9.2% lower from the planned dose distribution. Abbreviations are as in Fig. 1.

on dose distributions was likely greater than that of treatment machine errors calculated from log files after irradiation. According to previous reports, the geometric accuracy of TrueBeam, such as gantry or multileaf collimator (MLC) position, was found to be within 0.001 mm and 0.001°on an average [37].

A limitation for this study warrants discussion. Although mechanical uncertainties are small enough to perform STI with VMAT (Table 3), we did not incorporate these uncertainties into the resultant dose distributions. To calculate the dose closer to the actual delivered dose, it is necessary to develop a method that can take all factors affecting dose distribution into account.

Conclusion

In conclusion, the displacement of GTV position by intrafractional RSEs was independent of the distance between the isocenter and the GTV center position in STI with SI-VMAT for multiple brain metastases, despite GTVs being located far from the isocenter. The difference of $D_{0.5\%}$ between the planned and accumulated doses was within ±3.1%. Despite the difference of GTV $D_{99.5\%}$ and $D_{98\%}$ between the planned and accumulated values being >5% in some GTVs, there was no significant difference in $D_{99.5\%}$, $D_{98\%}$, and $D_{0.5\%}$. Note that, however, the aforementioned results were based on the fact that the intrafractional RSEs were reduced to a clinically acceptable level.

Declaration of Competing Interest

The authors declare that they have no known competing financial interests or personal relationships that could have appeared to influence the work reported in this paper.

Acknowledgements

We sincerely appreciate the technical support and guidance from all the staff members of the Medical Physics Laboratory of Kyoto University Graduate School of Medicine (http://medicalphysics.hs.med.kyoto-u.ac.jp/) provided throughout the study.

Funding

This work was supported in part by a JSPS Grant-in-Aid for Early-Career Scientists (Grant Number JP20K16723 and JP21K15548).

References

[1] Patchell RA. The management of brain metastases. Cancer Treat Rev 2003;29:533–40. https://doi.org/10.1016/s0305-7372(03)00105-1.
[2] Patchell RA, Tibbs PA, Regine WF, Dempsey RJ, Mohiuddin M, Kryscio RJ, et al. Postoperative radiotherapy in the treatment of single metastases to the brain: a randomized trial. JAMA 1998;280(17). https://doi.org/10.1001/jama.280.17.1485.
[3] Chang EL, Wefel JS, Hess KR, Allen PK, Lang FF, Kornguth DG, et al. Neurocognition in patients with brain metastases treated with radiosurgery or radiosurgery plus whole-brain irradiation: a randomised controlled trial. Lancet Oncol 2009;10(11):1037–44.
[4] Kepka L, Tyc-Szczepaniak D, Osowiecka K, Sprawka A, Trąbska-Kluch B, Czeremszynska B. Quality of life after whole brain radiotherapy compared with radiosurgery of the tumor bed: results from a randomized trial. Clin Transl Oncol 2018;20:150–9. https://doi.org/10.1007/s12094-017-1703-5.
[5] Wang C-W, Lin Y-C, Tseng H-M, Xiao F, Chen C-M, Cheng W-L, et al. Prolonged treatment time deteriorates positioning accuracy for stereotactic radiosurgery. PLoS One 2015;10(4):e0123359.
[6] Clark GM, Popple RA, Young PE, Fiveash JB. Feasibility of single-isocenter volumetric modulated arc radiosurgery for treatment of multiple brain metastases. Int J Radiat Oncol Biol Phys 2010;76:296–302. https://doi.org/10.1016/j.ijrobp.2009.05.029.
[7] Huang Y, Chin K, Robbins JR, Kim J, Li H, Amro H, et al. Radiosurgery of multiple brain metastases with single-isocenter dynamic conformal arcs (SIDCA). Radiother Oncol 2014;112(1):128–32.
[8] Ruggieri R, Naccarato S, Mazzola R, Ricchetti F, Corradini S, Fiorentino A, et al. Linac-based VMAT radiosurgery for multiple brain lesions: comparison between a conventional multi-isocenter approach and a new dedicated mono-isocenter technique. Radiat Oncol 2018;13:38. https://doi.org/10.1186/s13014-018-0985-2.
[9] AAPM Report Number 104. The role of in-room kV X-ray imaging for patient setup and target localization; 2009. https://doi.org/10.37206/104.
[10] Lightstone AW, Benedict SH, Bova FJ, Solberg TD, Stern RL. Intracranial stereotactic positioning systems: report of the American Association of Physicists in Medicine Radiation Therapy Committee Task Group No. 68: AAPM Task Group 68 Report. Med Phys 2005;32(7Part1):2380–98.
[11] Graulieres E, Kubler S, Martin E, Ferrand R. Positioning accuracy of a single-isocenter multiple targets SRS treatment: a comparison between Varian TrueBeam CBCT and Brainlab ExacTrac. Phys Med 2020;80:267–73. https://doi.org/10.1016/j.ejmp.2020.10.022.
[12] Gevaert T, Verellen D, Engels B, Depuydt T, Heuninckx K, Tournel K, et al. Clinical evaluation of a robotic 6-degree of freedom treatment couch for frameless radiosurgery. Int J Radiat Oncol Biol Phys 2012;83(1):467–74.
[13] Schmidhalter D, Fix MK, Wyss M, Schaer N, Munro P, Scheib S, et al. Evaluation of a new six degrees of freedom couch for radiation therapy. Med Phys 2013;40(11):111710.
[14] Mangesius J, Seppi T, Weigel R, Arnold CR, Vasiljevic D, Goebel G, et al. Intrafractional 6D head movement increases with time of mask fixation during stereotactic intracranial RT-sessions. Radiat Oncol 2019;14(1). https://doi.org/10.1186/s13014-019-1425-7.
[15] Roper J, Chanyavanich V, Betzel G, Switchenko J, Dhabaan A. Single-isocenter multiple-target stereotactic radiosurgery: risk of compromised coverage. Int J Radiat Oncol Biol Phys 2015;93:540–6. https://doi.org/10.1016/j.ijrobp.2015.07.2262.
[16] Prentou G, Pappas EP, Logothetis A, Koutsouveli E, Pantelis E, Papagiannis P, et al. Dosimetric impact of rotational errors on the quality of VMAT-SRS for multiple

brain metastases: comparison between single- and two-isocenter treatment planning techniques. J Appl Clin Med Phys 2020;21(3):32–44.
[17] Tsuruta Y, Nakata M, Nakamura M, Uto M, Takehana K, Hirashima H, et al. Evaluation of intrafractional head motion for intracranial stereotactic radiosurgery with a thermoplastic frameless mask and ceiling-floor-mounted image guidance device. Phys Med 2021;81:245–52.
[18] Kishi N, Nakamura M, Hirashima H, Mukumoto N, Takehana K, Uto M, et al. Validation of the clinical applicability of knowledge-based planning models in single-isocenter volumetric-modulated arc therapy for multiple brain metastases. J Appl Clin Med Phys 2020;21(10):141–50.
[19] TrueBeam Technical Reference Guide -Volume 2: Imaging. Available from: https//www.myvarian.com/s/.
[20] BRAINLAB EXACTRAC Clinical User Guide, Revision 1.2. Available from: https://userguides.brainlab.com/wp-content/uploads/2020/01/ExacTrac-6.5-CUG-English-60919-86EN-Rev.1.2.pdf.
[21] Rojas-López JA, Díaz Moreno RM, Venencia CD. Use of genetic algorithm for PTV optimization in single isocenter multiple metastases radiosurgery treatments with Brainlab Elements™. Phys Med 2021;86:82–90. https://doi.org/10.1016/j.ejmp.2021.05.031.
[22] Nakano H, Tanabe S, Utsunomiya S, Yamada T, Sasamoto R, Nakano T, et al. Effect of setup error in the single-isocenter technique on stereotactic radiosurgery for multiple brain metastases. J Appl Clin Med Phys 2020;21(12):155–65.
[23] Sagawa T, Ohira S, Ueda Y, Akino Y, Mizuno H, Matsumoto M, et al. Dosimetric effect of rotational setup errors in stereotactic radiosurgery with HyperArc for single and multiple brain metastases. J Appl Clin Med Phys 2019;20(10):84–91.
[24] Kraft J, van Timmeren JE, Mayinger M, Frei S, Borsky K, Stark LS, et al. Distance to isocenter is not associated with an increased risk for local failure in LINAC-based single-isocenter SRS or SRT for multiple brain metastases. Radiother Oncol 2021;159:168–75.
[25] Dupic G, Brun L, Molnar I, Leyrat B, Chassin V, Moreau J, et al. Significant correlation between gross tumor volume (GTV) D98% and local control in multifraction stereotactic radiotherapy (MF-SRT) for unresected brain metastases. Radiother Oncol 2021;154:260–8.
[26] Minniti G, Capone L, Alongi F, Figlia V, Nardiello B, El Gawhary R, et al. Initial experience with single-isocenter radiosurgery to target multiple brain metastases using an automated treatment planning software: clinical outcomes and optimal target volume margins strategy. Adv Radiat Oncol 2020;5(5):856–64.
[27] Palmiero AN, Critchfield L, St Clair W, Randall M, Pokhrel D. Single-isocenter volumetric modulated arc therapy (VMAT) radiosurgery for multiple brain metastases: potential loss of target(s) coverage due to isocenter misalignment. Cureus 2020;12:e11267. https://doi.org/10.7759/cureus.11267.
[28] Nataf F, Schlienger M, Liu Z, Foulquier JN, Grès B, Orthuon A, et al. Radiosurgery with or without a 2-mm margin for 93 single brain metastases. Int J Radiat Oncol Biol Phys 2008;70(3):766–72.
[29] Kirkpatrick JP, Wang Z, Sampson JH, McSherry F, Herndon JE, Allen KJ, et al. Defining the optimal planning target volume in image-guided stereotactic radiosurgery of brain metastases: results of a randomized trial. Int J Radiat Oncol Biol Phys 2015;91(1):100–8.
[30] Stern RL, Heaton R, Fraser MW, Murty Goddu S, Kirby TH, Lam KL, et al. Verification of monitor unit calculations for non-IMRT clinical radiotherapy: report of AAPM Task group 114. Med Phys 2011;38(1):504–30.
[31] Miften M, Olch A, Mihailidis D, Moran J, Pawlicki T, Molineu A, et al. Tolerance limits and methodologies for IMRT measurement-based verification QA: recommendations of AAPM Task Group No.218. Med Phys 2018;45(4):e53–83.
[32] Zhu TC, Stathakis S, Clark JR, Feng W, Georg D, Holmes SM, et al. Report of AAPM Task Group 219 on independent calculation-based dose/MU verification for IMRT. Med Phys 2021;48(10). https://doi.org/10.1002/mp.15069.
[33] Mijnheer B, Beddar S, Izewska J, Reft C. In vivo dosimetry in external beam radiotherapy. Med Phys 2013;40(7):070903.
[34] McCurdy BMC, McCowan PM. In vivo dosimetry for lung radiotherapy including SBRT. Phys Med 2017;44:123–30. https://doi.org/10.1016/j.ejmp.2017.05.065.
[35] Hirashima H, Nakamura M, Miyabe Y, Uto M, Nakamura K, Mizowaki T. Monitoring of mechanical errors and their dosimetric impact throughout the course of non-coplanar continuous volumetric-modulated arc therapy. Radiat Oncol 2018;13:27. https://doi.org/10.1186/s13014-018-0972-7.
[36] Olasolo-Alonso J, Vázquez-Galiñanes A, Pellejero-Pellejero S, Pérez-Azorín JF. Evaluation of MLC performance in VMAT and dynamic IMRT by log file analysis. Phys Med 2017;33:87–94. https://doi.org/10.1016/j.ejmp.2016.12.013.
[37] Wang R, Du Y, Yao K, Liu Z, Wang H, Yue H, et al. Halcyon clinical performance evaluation: a log file-based study in comparison with a C-arm Linac. Phys Med 2020;71:14–23.